

# Nascent starbursts in synchrotron-deficient galaxies with hot dust<sup>1</sup>

H. Roussel<sup>1</sup>, G. Helou<sup>1,5</sup>, R. Beck<sup>2</sup>, J.J. Condon<sup>3</sup>, A. Bosma<sup>4</sup>, K. Matthews<sup>1</sup>, and T.H. Jarrett<sup>5</sup>

1) *California Institute of Technology, Pasadena, CA 91125*

2) *Max-Planck Institut für Radioastronomie, 53121 Bonn, Germany*

3) *National Radio Astronomy Observatory, Charlottesville, VA 22903*

4) *Observatoire de Marseille, 2 place Le Verrier, 13248 Marseille cedex 4, France*

5) *Infrared Processing and Analysis Center, Pasadena, CA 91125*

hroussel@iraastro.caltech.edu

## ABSTRACT

Three nearby galaxies which have abnormally high infrared to radio continuum ratios, NGC 1377, IC 1953 and NGC 4491, are investigated with a view to understanding the physical origin of their peculiarity. We review the existing data and present new radio continuum measurements along with near-infrared integral-field spectroscopy and molecular gas observations. The three galaxies have low luminosities but starburst-like infrared colors; in NGC 1377, no synchrotron emission is detected at any wavelength; in IC 1953, the observed synchrotron component is attributable to the spiral disk alone, and is lacking in the central regions; the radio spectrum of NGC 4491 is unusually flat. We also compare and contrast them with NGC 4418, a heavily extinguished galaxy which shares some attributes with them. After examining various scenarios, we conclude that these galaxies are most likely observed within a few Myr of the onset of an intense star formation episode after being quiescent for at least  $\approx 100$  Myr. This starburst, while heating the dust, has not produced optical signatures nor a normal amount of cosmic rays yet. We briefly discuss the statistics of such galaxies and what they imply for star formation surveys.

*Subject headings:* galaxies: individual (NGC 1377, IC 1953, NGC 4491, NGC 4418)  
— infrared: galaxies — radio continuum: galaxies — supernova remnants

---

<sup>1</sup>Based on observations with the 100-m telescope of the Max-Planck Institut für Radioastronomie at Effelsberg.

## 1. Introduction

One of the implications from the data collected by the IRAS mission, combined with extensive radio surveys, is a nearly universal and tight correlation between the far-infrared thermal dust emission and the optically-thin total radio continuum emission (mixing thermal and synchrotron components) in normal star-forming galaxies. de Jong et al. (1985) have reached this conclusion comparing  $60\ \mu\text{m}$  fluxes with 6.3 cm fluxes from the Effelsberg dish, Helou et al. (1985) comparing 40–120  $\mu\text{m}$  fluxes with 21 cm fluxes from Westerbork. Although the correlation is generally expressed between luminosities, it holds when they are normalized to cancel size and distance effects, and is valid for a very broad range of star formation rate densities (review by Condon (1992)). At centimeter wavelengths, the radio emission is dominated by non-thermal processes.

All models accounting for the constancy of the infrared to radio flux ratios invoke the star formation process as the indirect source of both types of emission, via a production rate of cosmic rays by type-II supernovæ proportional to the production rate of heating photons. Additional coupling mechanisms are needed, such as between the interstellar medium density and the magnetic field intensity (Helou & Bica 1993), or between the star formation rate and the magnetic field amplification (Beck & Golla 1988; Niklas & Beck 1997). Various physical mechanisms can lead to these couplings, among which differential rotation, or turbulence driven by massive star formation amplifying the magnetic field. In addition, given that the various timescales involved in the underlying mechanisms are very different (heating of dust by massive and then intermediate-mass stars, explosion of supernovæ, acceleration, diffusion and decay of the relativistic electrons, variations of the magnetic field strength), some variation in infrared to radio flux ratios with the star formation recent history is to be expected.

There are naturally known exceptions to the general correlation. A fraction of galaxies hosting non-stellar nuclear activity have excess radio continuum emission, from cosmic rays accelerated in jets from the nucleus (Sopp & Alexander 1991; Roy et al. 1998). Star-forming galaxies in cluster environments can also have radio excess (Miller & Owen 2001), perhaps triggered by external magnetic field compression due to the intracluster gas pressure or to interactions with neighbor galaxies. Two pairs of colliding galaxies with excess synchrotron emission originating from a bridge between the disks were studied by Condon et al. (1993) and Condon et al. (2002b), to illustrate the importance to the correlation of regulated cosmic ray escape. Hummel & Beck (1995) also discovered excess synchrotron in an interacting galaxy, due to external compression of the magnetic field.

Some statistical studies found high far-infrared to radio ratios in compact galaxy groups (Menon 1991) and in lenticular galaxies (Walsh et al. 1989), but may suffer from photometric

errors (confusion problem for IRAS fluxes in galaxy groups, as pointed out by Sulentic & de Mello Rabaca (1993), and extended radio emission missed by interferometric observations).

For dwarf galaxies, metallicity effects can lower the dust emission, and the radio spectra of many are dominated by thermal emission. Wunderlich & Klein (1988) found that the far-infrared to radio ratio tends to be lower in blue compact galaxies than in spirals, while Klein et al. (1991) found similar ratios in both. Using the radio fluxes of Klein et al. (1991) and new IRAS fluxes measured with *Scanpi* (Helou et al. 1988), it seems in fact that there is a continuum of infrared to radio ratios from very low to very high values, i.e. with a much larger dispersion than in spirals, perhaps depending on two competing effects: reduction of the dust emission by metal deficiency, and reduction of the synchrotron emission by a lack of supernovæ or by fast escape of cosmic rays.

Variations also exist inside spiral galaxies: Beck & Golla (1988) found higher  $60\ \mu\text{m}$  to 11 cm flux ratios in the central regions of large angular size spirals than in their disks, following the  $F_{60}/F_{100}$  ratio, an average dust temperature indicator. This is likely because the scale length of the synchrotron emission is larger than in the infrared, due to cosmic ray propagation far from the site of their acceleration, located in star formation regions hosting hot dust (Bicay & Helou 1990; Marsh & Helou 1995).

In this paper, we study three nearby galaxies (an amorphous galaxy, an early-type spiral and a late-type spiral) which are strongly deficient in radio emission with respect to their dust emission, trying to identify the cause of their peculiarity. In normal galaxies, the synchrotron radiation comes mainly from electrons having left the supernova remnants which have accelerated them, and propagating in the interstellar magnetic field (Condon & Yin 1990). A lack of synchrotron emission may thus have its origin in either an unusually low strength of the magnetic field, or a reduced supernova rate in the recent past. With non-detections in the synchrotron emission, the magnetic field strength is extremely difficult to estimate. However, we address the star formation properties using an array of new observations, and thereby approach indirectly the issue of magnetic fields. We will argue that these galaxies have a high star formation rate associated with a low supernova rate, reflecting a starburst in a very early stage occurring after a long period of quiescence, since supernovæ begin to explode a few Myr after the birth of their progenitors.

If this interpretation is valid, these galaxies could provide the opportunity to observe the properties of the earliest stages of a starburst, and to understand better the regulation of the galactic infrared and radio emission. Although such galaxies are apparently quite rare, they may exist in greater numbers at more primitive epochs of star formation. They must therefore be taken into account when using high-redshift radio surveys to study the star formation history, and when using high-resolution radio observations to identify faint

infrared or submillimeter sources.

The paper is structured as follows: in Section 2 we discuss existing data and assemble comprehensive information about NGC 1377, IC 1953 and NGC 4491; Section 3 presents and analyses new radio continuum observations; in Section 4 we describe and exploit near-infrared spectroscopic observations, extract estimates of the star formation rate from the dust emission and discuss the excitation and apparent cooling rate of the interstellar medium; Section 5 examines results from single-dish molecular gas observations in NGC 1377; Section 6 is a brief discussion of some common properties of NGC 4418 with the three galaxies studied above; Section 7 lists and discusses the various physical scenarios which could account for the observed synchrotron deficiency. These scenarios are related either to a very low cosmic ray density stemming from a low supernova rate, or to a very low magnetic field intensity; we conclude in favor of the former, as would be expected in a nascent starburst. Section 8 then compares the statistics of synchrotron-deficient galaxies to those of nascent starbursts, and discusses possible triggering mechanisms. Section 9 contains a summary of our conclusions.

## 2. Descriptive review of the galaxies

General information about the three galaxies under consideration can be found in Table 1. NGC 1377 and IC 1953 were identified as radio synchrotron-deficient galaxies among the IRAS bright galaxy sample mapped with the VLA (Condon et al. 1990). NGC 4491, which is fainter, was also found to be synchrotron-deficient in a search among the small sample of Roussel et al. (2001b), based on mid-infrared colors (see Sect. 2.4). All three galaxies are low-mass and quite unremarkable at first sight, if it were not for their high dust temperatures. Being both faint and hot in their dust emission, they are very peculiar with respect to the average local  $L_{\text{FIR}}-F_{60}/F_{100}$  function, especially NGC 1377 (Chapman et al. 2002). The average  $F_{60}/F_{100}$  ratio at their infrared luminosities is only  $\approx 0.4$ , and they deviate from this by about  $10\sigma$  and  $5\sigma$ . Although IC 1953 seems to have a very close companion (Fig. 1), this galaxy is at much higher redshift (see Section 2.2).

### 2.1. Morphology

NGC 1377 is classified as a lenticular or amorphous galaxy, and does not present any apparent disturbance. Its only peculiarity, noted by Heisler & Vader (1994), is a central dust lane along the southern part of the minor axis, visible in the B-band isophotes. NGC 4491 is a barred dwarf Sa galaxy (Binggeli & Cameron 1983) whose shape is also regular, with

a tenuous outer disk. IC 1953 is a strongly barred Sd galaxy (the bar is short but straight and narrow, connecting at right angles to the spiral arms). It has an unusually bright and well-defined core for its late type (very prominent in the mid-infrared dust emission). One of the arms winds to join the opposite end of the bar, and the other arm, winding for more than  $360^\circ$ , offers the aspect of three distinct branches.

The mid-infrared emission of NGC 1377 and NGC 4491, in the ISOCAM maps at  $7\ \mu\text{m}$  and  $15\ \mu\text{m}$ , is dominated by the central regions, of apparent sizes respectively about 2.3 kpc and 800 pc, and the dust emission of IC 1953 is also more concentrated (in a 1.5 kpc region) than in other galaxies of its late-type morphology (Fig. 1). Decomposing the surface brightness profile of NGC 1377 at  $7\ \mu\text{m}$ , we find an unresolved source (at the resolution of ISOCAM, with a point spread function of  $\text{FWHM} = 5.7''$ ) contributing about 60% of the total flux or more. For NGC 4491, the central region is also unresolved in the mid-infrared, and superimposed onto a very diffuse component. The  $7\ \mu\text{m}$  brightness profile decomposition yields a point source accounting for about 65% of the flux of the infrared core, and 38% of the total flux. An unresolved source is also seen in the  $7\ \mu\text{m}$  brightness profile of IC 1953, containing about 65% of the flux of the circumnuclear regions.

## 2.2. Environment

NGC 1377 and IC 1953 are both members of the Eridanus galaxy group. According to Willmer et al. (1989), this is a small group (54 members brighter than  $B = 14.5$ ) in a young dynamical state, since it has an irregular and subclustered aspect, is rich in spiral galaxies, and forms with the Fornax cluster a bound system which is not yet virialized. In the soft X-ray maps of Burrows et al. (1993) (0.1–0.9 keV), Eridanus is not detected. NGC 1377 and IC 1953 do not belong to any subcondensation, but to the same loose sub-group lying in projection in the center, and are close to each other both spatially and in radial velocity.

NGC 4491 seems also to be part of a dynamically young system, the core named group A in the Virgo cluster, containing M 87 and 100 to 300 members, and which is described by Binggeli et al. (1993) as a “turbulent core with a long tail of low velocities”. NGC 4491 belongs to this tail, with a large velocity with respect to the systemic velocity of  $\approx -550\ \text{km s}^{-1}$ .

None of the three galaxies shows any morphological disturbance, but they have likely interacted with the ambient medium, since they are deficient in atomic gas. We did not find any published HI mass measurement for NGC 1377, but a spectrum from the HIPASS survey,

conducted with the Parkes telescope (Barnes et al. 2001).<sup>2</sup> This spectrum has a sensitivity of about 10 mJy per spectral channel, and implies that  $M(\text{HI}) < 2 \times 10^8 M_{\odot}$ . Compared with the S0/a-Sab galaxies in Guiderdoni & Rocca (1985), the logarithmic HI deficiency of NGC 1377, normalized by the dispersion in the field reference sample, is higher than 1.0. This value is  $def = 1.34$  for IC 1953 and  $def > 1.73$  for NGC 4491 (Roussel et al. 2001b), and a galaxy can be considered HI-deficient when  $def > 1.2$ .

IC 1953 has two small-mass neighbors, ESO 548-G040, a very low-surface brightness galaxy at about 2.6 arcmin in projected distance to the NW, and ESO 548-G036, at about 6 arcmin to the SE. ESO 548-G040 has a much higher receding velocity ( $4061 \text{ km s}^{-1}$ ) than the members of the Eridanus group ( $\approx 1600 \text{ km s}^{-1}$ ), and is therefore most likely a background galaxy. On the contrary, the velocity of ESO 548-G036 ( $1480 \text{ km s}^{-1}$ ) identifies it as a true neighbor of IC 1953, with a velocity difference of  $400 \text{ km s}^{-1}$  and a physical distance  $\geq 36 \text{ kpc}$ . It is thus tempting to consider ESO 548-G036 a candidate for tidal interaction with IC 1953, which could be responsible for the peculiar arm structure of IC 1953.

The closest neighbor to NGC 4491 is the blue compact dwarf IC 3446 at 6.3 arcmin to the W, and the closest galaxy of comparable mass is NGC 4497, at about 12 arcmin to the NW. Their velocities are  $760$  and  $610 \text{ km s}^{-1}$  larger than that of NGC 4491.

### 2.3. Far-infrared and radio properties

In order to build a reference for far-infrared to radio flux ratios, obtained with homogeneous IRAS and VLA data, we chose the sample of 69 nearby spiral galaxies studied by Roussel et al. (2001b), with mid-infrared and other data already at hand, and which comprises two of the three galaxies examined here, NGC 4491 and IC 1953. We measured IRAS fluxes using the *Scampi* tool (Helou et al. 1988) with default parameters. Only for NGC 4491 at  $100 \mu\text{m}$  was the baseline fitted over a  $30'$  range replaced by a baseline fitted over the central  $14'$  only, where it is reasonably flat. Given the brightness of the three target galaxies, we used as a flux estimator for them the template amplitude, except for IC 1953 which is slightly extended at  $25$  and  $60 \mu\text{m}$  (we used the flux integration of the scan between the first zero crossings). Radio continuum fluxes or upper limits at  $21 \text{ cm}$  were measured from NVSS maps (Condon et al. 1998), with a beam FWHM of  $45''$  and a detection limit of the order of  $1 \text{ mJy}$ . We obtain an upper limit for NGC 1377 which is equal to that given by the more

---

<sup>2</sup><http://www.atnf.csiro.au/research/multibeam/release/>. The Parkes telescope is part of the Australia Telescope which is funded by the Commonwealth of Australia for operation as a National Facility managed by CSIRO.

sensitive survey of Condon et al. (1990) in a 21''-beam.

Helou et al. (1985) defined a logarithmic ratio of far-infrared to radio flux densities as:  $q = \log [1.26 \times (2.58 F_{60} + F_{100}) / 3.75 \text{ (THz)} / S(21 \text{ cm})]$ , where all flux densities,  $F_{60}$ ,  $F_{100}$  and  $S(21 \text{ cm})$ , are expressed in the same unit. In the reference sample, excluding radio upper and lower limits, we find an average ratio  $\bar{q} = 2.34 \pm 0.19$ . The dispersion is the same as that obtained by Condon et al. (1991a) for the IRAS bright galaxy sample. The relationship between far-infrared and 21 cm fluxes, both normalized by the flux or the flux density in the blue band, is shown in Fig. 2. Five galaxies turn out to have far-infrared to radio flux ratios  $q > \bar{q} + 3\sigma$ : NGC 1377 ( $8.1\sigma$ ), NGC 4491 ( $5.5\sigma$ ) and IC 1953 ( $3.2\sigma$ ), with far-infrared to blue luminosity ratios higher than 1.5; NGC 4580 ( $3.9\sigma$ ) and NGC 4394 ( $3.2\sigma$ ), two Virgo galaxies having  $L_{\text{FIR}}/L_{\text{B}} < 0.25$ . The latter two are most clearly separated from the first three by their average dust temperature (Fig. 3): they have  $F_{60}/F_{100}$  of respectively 0.26 and 0.23, and also low mid-infrared colors  $F_{15}/F_7$  of 0.9 to 1, whereas NGC 4491 and IC 1953 have  $F_{60}/F_{100} = 0.8$ , and the flux density spectrum of NGC 1377 peaks at  $60 \mu\text{m}$ .

The lack of radio synchrotron emission can be accounted for easily in the cool-dust galaxies. If their star formation rate is presently very low, as indicated by their dust emission properties (low colors and low surface brightnesses), then the far-infrared-emitting dust can be expected to be heated mainly by low-mass stars, well in excess of the emission produced by the star formation activity. After the production of cosmic rays has ceased, the timescale for synchrotron emission decay is less than  $10^8$  years (Condon 1992), so that the  $q$  ratio should increase on this timescale after an exhaustion of the star formation. The whole disk of NGC 4394 is extremely diffuse in  $\text{H}\alpha$  (Koopmann et al. 2001) and in the mid-infrared as well (Roussel et al. 2001a). This is true also of NGC 4580 outside its inner pseudo-ring. However, the high  $F_{60}/F_{100}$  ratios of NGC 1377, NGC 4491 and IC 1953 exclude such an explanation for their lack of synchrotron emission.

The correlation between far-infrared and radio continuum luminosities is known to be non-linear, the radio emission rising faster or decreasing faster than the dust emission (Dereverux & Eales 1989). Faint galaxies such as those studied here are thus expected to have higher  $q$  ratios than brighter galaxies. However, Hummel et al. (1988) found evidence of a small decrease of  $F_{100}/S(20 \text{ cm})$  when the average dust temperature  $F_{60}/F_{100}$  rises, along with an increase of the radio brightness temperature. To linearize and tighten the relationship between infrared and radio fluxes, Condon et al. (1991a) apply an empirical correction which assumes that the radio emission is a good measure of the star formation rate, and decreases the  $q$  ratio in proportion to  $q_{\text{b}} = F_{\text{B}}/S(20 \text{ cm})$ , the blue to radio flux ratio. Although they find that variations in  $F_{60}/F_{100}$  cannot account for the dispersion in  $q$ ,  $F_{60}/F_{100}$  is correlated with  $q_{\text{b}}$ , and the trend of decreasing  $q$  with increasing  $F_{60}/F_{100}$  exists in our

sample also (particularly illustrated in Fig. 3 by the behavior of NGC 4580 and NGC 4394). NGC 1377, NGC 4491 and IC 1953 manifestly break this trend. If we apply the correction of Condon et al. (1991a) to our data, as shown in Fig. 4, then the peculiarity of NGC 1377, NGC 4491 and IC 1953 with respect to the other galaxies is not destroyed: they still lie at  $5.9\sigma$ ,  $3.6\sigma$  and  $2.4\sigma$  above the new mean  $q_c = 2.22 \pm 0.18$ . The only other galaxy having  $q_c > \bar{q}_c + 2\sigma$  is NGC 1022 ( $q_c = \bar{q}_c + 2.5\sigma$ ), an amorphous starburst with  $F_{60}/F_{100} = 0.76$ . We note that the correction proposed by Devereux & Eales (1989), based on the blue to infrared luminosity ratio, cannot be appropriate, since  $q$  as a function of  $L_B/L_{\text{FIR}}$  shows no defined trend.

The high  $F_{60}/F_{100}$  and low  $F_{12}/F_{25}$  ratios signal the existence of a dust component with high temperatures and thus high heating intensities, which could be due to an extensive star formation burst or non-stellar activity, or both (Helou 1986). In this respect, the spectral indices between 25 and 60  $\mu\text{m}$  of NGC 1377 and NGC 4491, -1.5 and -2.1, are ambiguous (de Grijp et al. 1987).

## 2.4. Spectral energy distribution and power source

The broadband spectral energy distributions of the three galaxies are shown in Fig. 5. J, H and Ks-band fluxes are derived from images built for the 2MASS Large Galaxy Atlas (Jarrett et al. 2003), with a preliminary photometric calibration valid for the CIT system. The U, V and I-band fluxes of NGC 1377 come from the colors given by Heisler & Vader (1994). Other optical data were found in the NED database. We measured the 4–5  $\mu\text{m}$  fluxes of NGC 1377 and IC 1953 in ISOCAM maps.

It appears that the dust emission spectrum of NGC 1377 cannot be reproduced by any empirical SED of Dale et al. (2001) (Fig. 5), adjusted to a sample of normal galaxies, and parametrized by the  $F_{60}/F_{100}$  ratio (note however that the color bin of NGC 1377 comprises only two galaxies). The emission from transiently-heated dust particles, from 7 to 25  $\mu\text{m}$ , is well in excess of what is expected for the large grain temperature (as estimated by the  $F_{60}/F_{100}$  ratio), by up to  $8\text{--}9\sigma$ .  $L_7/L_{\text{FIR}}$  is expected to decrease steadily with rising dust temperature, and then starts to increase again at the highest  $F_{60}/F_{100}$  ratios, but NGC 1377 overdevelops this trend (Fig. 6). For  $F_{15}/F_{\text{FIR}}$ , which in normal galaxies shows less dispersion than  $F_7/F_{\text{FIR}}$ , the same remark applies.

The mid-infrared spectral shape between 2.5 and 11  $\mu\text{m}$ , observed with ISOPHOT in  $24'' \times 24''$  Laureijs et al. (2000), is quite unusual: instead of the typical spectrum of aromatic bands observed in most star-forming galaxies (Helou et al. 2000), a broad asymmetric feature



between 6 and  $8.5\ \mu\text{m}$  contributes the bulk of the emission. This is reminiscent of some ultraluminous galaxies (Rigopoulou et al. 1999; Tran et al. 2001). Such a broad feature, accompanied by very weak  $6.2$  and  $11.3\ \mu\text{m}$  bands, is also observed in the peak E of the SMC HII region N66 by Contursi et al. (2000), in proto-planetary nebulae (Kwok et al. 2001), and bears some resemblance with the signature of anthracite, used by Guillois et al. (1996) to reproduce proto-planetary nebula spectra. All this suggests that the aromatic band carriers have not been processed in the same way as in normal star-forming galaxies, and that the dust responsible for the emission is subjected to hard radiation. Since it contributes the same part in the infrared energy budget as in quiescent galaxies, this dust must be more resilient in order not to be destroyed. The abrupt fall-off of the spectrum from  $9$  to  $11\ \mu\text{m}$  further suggests that the absorption by silicates may be substantial, but such an interpretation is very hazardous, because optically-thin spectra of normal galaxies also have a minimum in this region. Dust heating cannot be provided by a shock, in particular because one would then observe either a prominent silicate emission feature, or a negligible mid-infrared emission with respect to the far-infrared emission, depending on the gas density (Draine 1981; Dwek et al. 1996).

Laureijs et al. (2000), on the basis of this spectrum, propose that NGC 1377 contains a buried Seyfert nucleus. However, several arguments suggest otherwise:

1) The continuum emission at  $3\text{--}4\ \mu\text{m}$  and  $9\text{--}11\ \mu\text{m}$  is near zero, contrary to what is observed in Seyfert nuclei. The short-wavelength continuum, in particular, which is not affected as much by extinction, is now routinely used as a diagnostic of the contribution of an active nucleus to the energy budget (Genzel et al. 1998; Laurent et al. 2000). Among the sample of Laureijs et al. (2000), the spectrum of NGC 1377 resembles much more that of IRAS 02530+0211, a galaxy of starburst type, than that of any of the Seyfert galaxies. One could argue that the broad feature seen between  $6$  and  $8.5\ \mu\text{m}$  is similar to that seen in Centaurus A (Laurent et al. 2000), and is produced by a continuum strongly absorbed longward of  $8\ \mu\text{m}$  by silicates; however, the similarity is superficial, since the spectra of Centaurus A and other Seyfert nuclei rise steeply longward of  $10\ \mu\text{m}$  and are brighter at  $11.5\ \mu\text{m}$  than at  $8\ \mu\text{m}$ , whereas the  $11.5\ \mu\text{m}$  flux of NGC 1377 is near zero. This is a strong argument against pure silicate absorption, because the red wing of the absorption band would otherwise be exceptionally wide. Trying a quantitative fit of the  $8\ \mu\text{m}$  to  $100\ \mu\text{m}$  data, with the extinction law of Draine & Lee (1984) (some variants exist, but introduce differences essentially shortward of  $8\ \mu\text{m}$ , which is why we exclude short wavelengths),  $A_V \approx 70$  is required in order to reproduce the  $8\text{--}10\ \mu\text{m}$  ISOPHOT spectrum with an absorbed dust continuum, but no good fit can be performed: the solution is too high in the  $10\text{--}11.5\ \mu\text{m}$  range; one can obtain a simultaneous fit of the  $12\ \mu\text{m}$ ,  $25\ \mu\text{m}$ ,  $60\ \mu\text{m}$  and  $100\ \mu\text{m}$  data with the sum of two blackbodies of  $370\ \text{K}$  and  $100\ \text{K}$ , but the fit at  $15\ \mu\text{m}$  is then much higher than the observed

flux, which is impossible to fix by adding a new dust component. We thus conclude that the broad feature between 6 and  $8.5\ \mu\text{m}$  may contain a genuine emission band, and may not be exclusively caused by absorption<sup>3</sup>.

**2)** The J, H and K-band surface brightness profiles computed by Heisler et al. (1996) are nearly flat inside the central 3–4'', significantly below the best  $r^{1/4}$  fit, whereas most Seyfert galaxies with  $F_{60} > F_{100}$  require an extra nuclear point source. A high central absorption could flatten the profiles, but this is unlikely, because 2MASS data indicate that the J-H and H-K colors of the central 10'' are not different from the global colors within the error bars. H-K is relatively “blue” compared to the other galaxies in Heisler et al. (1996), and J-K is very blue compared to the ultraluminous galaxies in Klaas et al. (2001) (like the bluest starbursts and Liners), or to the 2MASS extended sources brighter than  $K_s = 14$  (Jarrett 2000; Jarrett et al. 2003). The power emitted by dust between 4.5 and  $100\ \mu\text{m}$  is only 1.8 times the total stellar power between  $3600\ \text{\AA}$  and  $4.5\ \mu\text{m}$ , and about twice more considering the center alone. This means that the luminosity-weighted extinction cannot be high enough to hide a deep stellar potential well.

**3)** Seyfert galaxies either emit excess radio emission with respect to their infrared emission, or follow the same correlation as normal galaxies (Sopp & Alexander 1991). Although no starburst galaxy is known to be as radio-deficient as NGC 1377, no active nucleus either has been shown to be synchrotron-deficient so far. X-ray data would be useful to rule out Seyfert activity, but to our knowledge, none exist for NGC 1377.

The 7 to  $25\ \mu\text{m}$  emission of NGC 4491 is somewhat in excess of the corresponding SED of Dale et al. (2001), but not significantly. The blue-band surface brightness profile of Kodaira et al. (1986) is exponential, with no central peak, and so are the near-infrared profiles. The J-H and H-K colors are close to those of NGC 1377, and the color differences between the circumnuclear region and the whole galaxy are small. The same conclusions thus apply.

As to IC 1953, only the  $7\ \mu\text{m}$  emission is  $2\ \sigma$  in excess of the average empirical SED. Its global near-infrared colors are extremely blue, and its circumnuclear colors are slightly bluer than those of NGC 1377 and NGC 4491. Since the disk infrared emission in IC 1953 is significant, and well resolved in ISOCAM maps, we decomposed the spectral energy distribution into a disk component and a circumnuclear region (CNR) component, which we identify to

---

<sup>3</sup>Note that if  $A_V = 70$  is adopted, then the emission of hot small grains up to  $\approx 25\ \mu\text{m}$  would have to be boosted by a factor five to obtain the intrinsic small grain luminosity. Since the complementary power observed in the far-infrared is only 1.2 times the observed power of small grains, at least  $3L_{\text{FIR}}$  would have to be re-emitted at longer wavelengths, in the submillimeter, which is inconceivable. And this would only exacerbate the difficulty to account for the dust luminosity of NGC 1377 in the total absence of activity in the radio window (this will be developed in Sect. 7.5).

the core with a high  $F_{15}/F_7$  ratio. To do this, we estimated typical disk infrared colors using the ISOCAM and IRAS fluxes of NGC 4027 (Roussel et al. 2001a), which has high signal to noise ratios and whose entire body can be assimilated to a disk:  $F_{15}/F_7 = 0.87$  (the small  $7\ \mu\text{m}$  excess in the disk of IC 1953 being ascribed to stellar emission),  $F_{12}/F_7 = 0.85$ ,  $F_{25}/F_7 = 1.37$ ,  $F_{60}/F_7 = 13.2$  and  $F_{100}/F_7 = 37.7$ . The result, shown in Fig. 5d, outlines the fact that part of the peculiarity of IC 1953 is hidden by normal disk properties: the center has hotter dust and higher infrared to optical ratios than the galaxy as a whole. The radio deficiency is likely more severe in the center; using the radio measurement of Condon et al. (1990) inside  $21''$  and the above decomposition, we obtain  $q_{\text{CNR}} = 3.44 = \bar{q} + 5.7\sigma$ .

The position of a galaxy in a mid-infrared surface brightness–color diagram ( $\Sigma(15\ \mu\text{m})$  versus  $F_{15}/F_7$ ) can give some sense of the relative contribution of stellar populations of different ages, on a timescale of several  $10^8$  years, in the dust heating (Roussel et al. 2001b). The circumnuclear regions of NGC 4491 and IC 1953 populate a part of the diagram otherwise empty<sup>4</sup>, and have a central  $F_{15}/F_7$  color more than twice the average value corresponding to their surface brightness. This is fully consistent with the hypothesis that they are undergoing a starburst in an early phase, which is massive with respect to the mass of the underlying intermediate stellar population. As for NGC 1377, its  $F_{15}/F_7$  excess is only moderate. However, the emission in the  $7\ \mu\text{m}$  bandpass being due to an unusual dust species, the interpretation of its  $F_{15}/F_7$  color is not straightforward.

### 3. Multi-wavelength radio continuum

We mapped the galaxies with the Effelsberg 100 m antenna<sup>5</sup>, at 6.2 cm and 3.6 cm, during six observation sessions between April and August 2002. These observations made use of the 4850 MHz HEMT dual-horn receiver (30 K system temperature, 500 MHz bandwidth) and the 8350 MHz HEMT single-horn receiver (25 K system temperature, 1100 MHz bandwidth), both installed in the secondary focus of the telescope. The beamwidths are  $147''$  at 6.2 cm and  $82''$  at 3.6 cm, thus comparable to the galactic disk sizes. Between 10 and 20 coverages per galaxy were obtained, scanned in azimuthal direction at 6.2 cm and in right ascension and declination, alternatively, at 3.6 cm. 3C138 and 3C286 were used as flux calibration sources. The data reduction was performed using the NOD2 software package. The coverages were

---

<sup>4</sup>The only other galaxies in the same part of the diagram are NGC 4388, a Seyfert galaxy, and NGC 4519, a galaxy akin to IC 1953 in many respects, but whose peculiar central regions may be diluted in the emission of its bright disk.

<sup>5</sup>The Effelsberg telescope is operated by the MPIfR Bonn on behalf of the Max-Planck-Gesellschaft e.V.

combined by applying the “basket-weaving” technique (Emerson & Gräve 1988). The final 3.6 cm maps were smoothed to a beamwidth of  $90''$  to increase the signal to noise ratio.

The measured flux densities are contained in Table 4 and the contour maps shown in Fig. 7. Significantly polarized emission was not detected in any galaxy. Figure 8 compares the radio measurements with the free-free and synchrotron spectra of normal galaxies matched to the far-infrared fluxes of NGC 1377, IC 1953 and NGC 4491. The total flux expected at 21 cm was derived from the average  $q$  ratio, the free-free component from the ionizing photon flux estimate (assuming  $T_e = 5000$  K), and we adopted the spectral indices  $S_{\text{sync}} \propto \nu^{-0.75}$  and  $S_{\text{ff}} \propto \nu^{-0.1}$ , unless otherwise constrained for the synchrotron component.

### 3.1. NGC 1377

NGC 1377 is not detected at any radio frequency, and the upper limits even lie below fluxes expected from a mere free-free component matched to the ionizing photon flux derived from the dust emission (Fig. 8). This fact suggests to us not only that NGC 1377 is mostly devoid of synchrotron radiation, but also that the star formation episode is so young that most massive stars are still embedded in their parent molecular clouds, which would cause a large fraction of the ionizing photons to be intercepted by dust before being able to ionize the gas. NGC 1377 was reobserved in 1990 at 3.55 cm with the VLA in the A configuration, yielding a beam of  $0.4'' \times 0.25''$  (J.J. Condon, unpublished). The galaxy is still undetected at this high resolution, and the  $3\sigma$  upper limit is 0.13 mJy per beam, i.e. 15 times less than the 3.6 cm upper limit from Effelsberg. Interpreting this limit, we have to take into account the possibility that the star-forming region be more extended than  $0.3''$ . Assuming a size of 100 pc or  $\approx 1''$  (see the next to last paragraph in this section), the equivalent upper limit on the total 3.55 cm flux is of the order of 1.3 mJy. Vader et al. (1993) derive from a “snapshot” observation with the VLA  $S(6 \text{ cm}) < 0.9$  mJy for NGC 1377, in a  $4''$ -beam, which brings a stronger constraint. In such conditions, the data require a reduction of ionizing photons by about 70% or more (also by 70% using instead the 21 cm upper limit). If we adopt the limit in a  $0.3''$ -beam, then the ionizing photons have to be suppressed by more than 95%. If indeed a larger fraction than usual of the ionizing photons are absorbed by dust in NGC 1377, then this will have the simultaneous effect of decreasing the free-free emission and enhancing the infrared emission, with respect to a normal galaxy with the same star formation rate.

Thermal opacity is an alternative explanation for the non-detection of the free-free emission. The upper limit at 3.55 cm however places very stringent a constraint in this case: with  $S(3.55 \text{ cm}) < 1.3$  mJy, the effective opacity is  $\tau(3.6 \text{ cm}) > 0.83$ , or  $\tau(21 \text{ cm}) > 31$ . Assuming a simple geometry and uniform electronic density, such a value would imply that

the scale of the emitting region be less than 28 pc, and the electronic density higher than  $2700 \text{ cm}^{-3}$ . Since this is unrealistic, the free-free opacity explanation is dismissed.

Assuming a normal initial mass function and no dust emission excess, the starburst must have produced approximately  $10^4$  O stars (see Section 4.2). Assuming that the dust emission at 60 and  $100 \mu\text{m}$  is due to a pure blackbody of temperature 80 K (which fits the 25 to  $100 \mu\text{m}$  data with only a small observed excess of 25% at  $25 \mu\text{m}$ ), its diameter is about 37 pc. Using the model of Désert et al. (1990) for O5 stars, the size of the starburst region is rather of the order of 100 pc ( $1''$ ) or larger. The emission region may thus be truly more extended than the VLA A-configuration beam. To trigger star formation quasi-instantaneously over such a scale perhaps needs a merger with a satellite galaxy, which does not necessarily produce morphological disturbances, but should be visible in the gas kinematics.

The dust mass required to produce the observed far-infrared emission is  $\approx 2.7 \times 10^5 M_\odot$ , according to the dust emissivity derived by Bianchi et al. (1999) for the Galaxy, with  $T_{\text{dust}} = 54 \text{ K}$  (which produces an emission excess from small dust grains of 76% at  $25 \mu\text{m}$ ). Using instead a blackbody fit, only  $4.0 \times 10^4 M_\odot$  of dust are needed. Assuming that the gas to dust mass ratio is similar to the Galactic value of  $\approx 100$  (Sodroski et al. 1994), the gas mass associated with the starburst in NGC 1377 is then of the order of  $4 \times 10^6$  to  $3 \times 10^7 M_\odot$ , which represents much less than 10% of the observed stellar mass in the whole central region. Since this mass ratio is reasonable, the hypothesis that the dust is heated by a starburst is plausible, but still needs to be confirmed by observations of the molecular gas: see Section 5. The upper limit on the atomic gas mass,  $M(\text{HI}) < 2 \times 10^8 M_\odot$  (Section 2.2), is not in contradiction with the starburst hypothesis. We will discuss the possibility that a radio-quiet active nucleus heats the dust in Section 7.5.

### 3.2. IC 1953

The entire radio spectrum lies well below a normal synchrotron spectrum, but contrary to NGC 1377, it is higher than the expected free-free component alone. At 21 cm, Condon et al. (1990) measure a flux density of  $\approx 2 - 3 \text{ mJy}$  inside a  $21''$ -beam, which is a bit larger than the size of the circumnuclear regions seen in the mid-infrared. This value is consistent with the free-free emission derived from the infrared spectrum of the central regions. As explained in Section 2.4, we performed a decomposition of the infrared spectral energy distribution into disk and circumnuclear (CNR) components, based on an empirical color model and on the true distribution observed at 7 and  $15 \mu\text{m}$ . This allows us to estimate the free-free and synchrotron emission separately for the disk and the galactic center, as shown in Fig. 8 (note that no component has been tuned in any way to the radio data in this graphic).

The central regions thus appear almost devoid of any synchrotron emission; otherwise, the 21'' measurement would be higher. This finds support in the total flux densities at 21 cm, 6.2 cm and 3.6 cm being in agreement with the synchrotron radiation derived for the disk alone (with a reasonable spectral index assumed for illustration purposes to be -0.75). Extremely diffuse extended emission from the disk is detected at all three wavelengths. The 3.6 cm map contains extensions to the south, which do not correspond to any structure at other wavelengths and are thus suspect; if the flux measurement is limited to the beam area rather than the total extension, however, then one obtains  $2.4 \pm 1.0$  mJy instead of  $3.6 \pm 2.2$  mJy. The data therefore are consistent with free-free emission and disk synchrotron emission, but not with the central synchrotron component expected from a normal supernova rate. One may question this result, since a minimum level of emission would be produced by cosmic rays originating in the disk and diffusing into the central region. In  $10^7$  years, cosmic rays may propagate to about 1 kpc from their source, using a diffusion coefficient of a few  $10^{24} \text{ m}^2 \text{ s}^{-1}$ , as found by e.g. Strong (1977) and Wallace (1980) in the Galaxy. Scaling the disk synchrotron brightness, which is very low, by a reasonably large size of 5'' for the starburst, and by an increase of the magnetic field strength from  $10 \mu\text{G}$  to  $50 \mu\text{G}$  (see Section 7.3 for a justification of these numbers), we estimate the synchrotron emission from disk cosmic rays to be at most of the same order as the free-free emission within the central region, even at 20 cm. Furthermore, if the central magnetic field is much larger than the disk magnetic field, then it will reflect cosmic rays coming from the disk (Fermi 1954).

IC 1953 was reobserved at 3.55 cm with the VLA in the A configuration ( $0.4'' \times 0.25''$  beam). The detected flux is  $0.80 \pm 0.05$  mJy, and the size of the emitting region of the order of  $0.17'' \times 0.09''$ , with a position angle of  $11^\circ$  (J.J. Condon, unpublished). This compact component accounts for less than half the peak flux density measured at 3.6 cm with the Effelsberg antenna, which is  $2.0 \pm 0.6$  mJy. It is consistent with normal free-free emission provided that about 65% of the flux comes from a region larger than  $0.3''$ , i.e. 30 pc, which is very likely, since the lower limit on the size of the starburst, obtained for a blackbody of 70 K matched to the CNR far-infrared emission, is 46 pc.

### 3.3. NGC 4491

Only for NGC 4491 does a flux measurement at another radio wavelength exist. Niklas et al. (1995) measured  $S(2.8 \text{ cm}) = 5 \pm 1$  mJy, with the Effelsberg telescope, in a  $69''$ -beam. Since the observed flux density at 3.6 cm in NGC 4491 ( $5.0 \pm 0.3$  mJy), confirming the measurement of Niklas et al. (1995) at 2.8 cm, is in good agreement with what is expected from the spectra of normal galaxies (4.9 mJy for a non-thermal index of -0.75 between 3.6 cm

and 21 cm), and the free-free emission can contribute only of the order of 20% of the total emission at this wavelength, we have evidence that NGC 4491 produces synchrotron emission. However, this emission seems to vanish at 21 cm: the NVSS map indicates that  $S(20\text{ cm}) < 1.35\text{ mJy}$ . NGC 4491 was not detected either in the (much less sensitive) 12.6 cm survey of Dressel & Condon (1978). Source confusion could be responsible for this inconsistency. Using the 8.4 GHz source counts of Fomalont et al. (2002), which indicate  $9 \times 10^{-4} < N(S > 4\text{ mJy})(\text{arcmin}^{-2}) < 2 \times 10^{-3}$ , and a beam of  $80''$ , the probability of observing a confusing source at 3.6 cm lies between 1/360 and 1/800. Given that the radio positions at 3.6 cm and 6.2 cm are in good agreement with the optical center, as well as the position at 6.2 cm of a bright quasar seen to the SW in the NVSS map, and that the observed flux coincides with the flux expected from the infrared emission, confusion is unlikely.

As NGC 4491 lies only  $54.5'$  away from M 87, which emits about 220 Jy at 20 cm, it is possible that the NVSS map does not retrieve the correct flux density of NGC 4491, due to imperfect cleaning of the beam sidelobes which can generate negative sources. To evaluate this effect, we selected a random sample of 50 NVSS fields (centered on NED extragalactic sources), at distances to M 87 between  $52.5'$  and  $56.5'$ , and looked in each one for the minimum brightness. The histogram of the minima forms a smooth distribution down to  $-6.52\text{ mJy}$  per beam, and two outliers at  $\approx -12$  and  $-16\text{ mJy}$  per beam. The latter are characteristically associated with a chain of other deep negative points, of amplitude scaled by about one third. Since this pattern is not present in the NGC 4491 map, we are confident that such a deep negative component cannot be superimposed onto NGC 4491 (furthermore, it would have to coincide accurately with the galaxy's position, the probability of which is low). We thus adopt as an absolute upper limit to any missing flux density the value  $6.52\text{ mJy}$ , and we derive  $S(20\text{ cm}) < 7.9\text{ mJy}$ . We will use this limit in the following discussion, but we insist that deeper observations at 20 cm are needed to set any more significant limit.

The new infrared to radio flux ratio is only constrained to be  $q > 2.65 = \bar{q} + 1.6\sigma$ . However, the spectral indices are very flat:  $S([3.6\text{--}6.2\text{ cm}]) \propto \nu^{-0.34}$  and  $S([6.2\text{--}20\text{ cm}]) \propto \nu^\alpha$  with  $\alpha > -0.22$ . The second value is very uncertain, but the  $[3.6\text{--}6.2\text{ cm}]$  index is more reliable. From radio continuum studies carried out at high angular resolution (Tarchi et al. 2000; Beck et al. 2000; Turner et al. 1998; Koblunicky & Johnson 1999), several starburst galaxies, e.g. NGC 2146, NGC 4214, NGC 5253, He 2-10 – for the most part with Wolf-Rayet signatures and being either irregular, amorphous, blue compact or merging dwarf galaxies – have been found to contain sources with flat or inverted radio spectra, revealing optically-thick free-free emission regions. However, we find that considering *total* infrared and radio fluxes, all of these galaxies have normal  $q$  ratios (between 2.23 and 2.67). Moreover, NGC 4491 emitting synchrotron emission at 3.6 cm, it is much more difficult to explain the shape of its radio spectrum by free-free absorption, for the thermal electrons would have to

fill a very compact distribution, and at the same time encompass the relativistic electrons. Assuming nevertheless that this is the case, the effective opacity at 20 cm would have to be larger than 0.7. Condon et al. (1991b) found three ultraluminous galaxies with  $q > 2.9$ , which are argued to be compact starbursts in merging systems, and whose radio-quiescence is best explained by high free-free opacity. However, these very luminous objects are not comparable at all with the galaxies studied here. For two of them do stellar continuum observations exist, and their  $60\ \mu\text{m}$  to near-infrared power ratios are more than 20 to 40 times greater than in NGC 1377, NGC 4491 and IC 1953. Furthermore, the required free-free opacities are only 0.5–0.7 at 20 cm. Thus, NGC 4491 is more likely intrinsically deficient in synchrotron emission rather than opaque at 20 cm.

The hypothesis of non-stellar activity powering the infrared and radio emission will be discussed in Section 7.5. Another possibility is that the population of relativistic electrons is very young, so that no significant energy losses occurred yet. We address here the likelihood of such a scenario. The median spectral index of radio supernova remnants, which are the likely sites of cosmic ray acceleration, is about  $-0.5$  (with a total distribution between  $-0.2$  and  $-0.8$ ), independent of age (Clark & Caswell 1976; Gordon et al. 1999). This is significantly flatter than the spectral index of diffuse synchrotron emission in galactic disks,  $-0.8$  on average (Niklas et al. 1997). Very flat indices of supernova remnants can be reproduced in diffusive shock acceleration models, when second-order Fermi acceleration is also included (Dröge et al. 1987) or when backreaction on the shock due to the pressure of the relativistic particles is taken into account (Pelletier & Roland 1988). Since the lifetime of radio supernova remnants is short,  $\approx 10^5$  years (Ulvestad 1982), and they normally account for a small fraction of the total synchrotron emission in a galaxy, it is unrealistic to assume that the radio continuum emission of NGC 4491 be due predominantly to flat-spectrum supernova remnants. Steepening of the energy spectrum is a natural effect of synchrotron and inverse Compton losses, once the relativistic electrons have escaped their acceleration sites, but it gradually takes place over their whole lifetime of several  $10^7$  years. Cosmic-ray diffusion also contributes to steepen the radio spectrum: with a diffusion length scaling as  $E^{-0.6}$  for  $E > 1.5\ \text{GeV}$  (Engelmann et al. 1990), the spectral index is decreased by  $-0.3$ .

The flat radio spectrum of NGC 4491 can therefore be explained if any old population of cosmic rays has completely decayed, and a fresh population has started building up within the last few Myr. This is consistent with the observations presented in Section 4.1.1. Assuming constant spectral indices between each measurement pair, the total radio power of NGC 4491 between 3.6 cm and 20 cm is of the order of 74% of the radio power expected of a normal spectrum, or less, owing to the 20 cm upper limit and to the fact that unobserved frequencies lower than 1.4 GHz were not included in the computed power. It is thus conceivable that not all cosmic rays were yet released by supernova remnants and that the interstellar medium



of NGC 4491 is out of equilibrium (in which case the assumption of equipartition between cosmic ray and magnetic energy densities is invalidated).

#### 4. Star formation indicators

The  $H\alpha$  recombination line, classically used as tracer of massive stars, is not suitable to estimate the star formation rates of the three galaxies, because nebular extinction in the circumnuclear core can be expected to be high. In a  $2''$ -wide slit placed on the nucleus of NGC 1377, Kim et al. (1995) detect [NII] (6583 Å) and [SII] (6716 and 6731 Å) in emission, but not  $H\alpha$ , and furthermore a high [SII]<sub>6716</sub> to [SII]<sub>6731</sub> ratio, indicating that the detected nebular emission arises in low-excitation and low electronic density regions, presumably in shocks. Modelling the starburst nucleus of NGC 4569, Gabel & Bruhweiler (2002) found that the [SII] and [NII] emission arises predominantly from low-density gas at large distances from the starburst core; the same may apply to NGC 1377.

IC 1953 was observed in ( $H\alpha$  + [NII]) by García-Barreto et al. (1996), who kindly provided their map to us. In the  $H\alpha$  light, the circumnuclear region is fainter than several star-formation complexes in the disk, whereas it is of much higher surface brightness than any other part of the galaxy in the 7 and 15  $\mu\text{m}$  dust emission. The bar is not detected in  $H\alpha$ , which is not customary in late-type galaxies, but more characteristic of strong bars.

The three galaxies do not feature in the optical range any indication of a starburst, but have starburst-like far-infrared and mid-infrared colors. In order to better constrain the star formation and supernova rates, we undertook an observation program of near-infrared emission lines.

##### 4.1. Near-infrared spectroscopy

We observed NGC 4491 on February 1 and 2, 2002, at the 5-m Hale telescope at the Palomar observatory, with the Palomar Integral Field Spectrograph, PIFS (Murphy et al. 1999). The hydrogen recombination lines  $\text{Pa}\beta$  and  $\text{Br}\gamma$  were chosen to estimate the star formation rate and the extinction in the circumnuclear region, and the [FeII] 1.644 line was used to set a constraint on the supernova rate. We also observed NGC 4102, as a bright comparison galaxy with a very young circumnuclear starburst (Jogee & Kenney 1995; Roussel et al. 2001b), but normal infrared and radio properties; its  $q$  ratio is 2.37, and its central mid-infrared color,  $F_{15}/F_7 = 3.1$ , is comparable to those of the three galaxies studied here. On October 17-19, 2002, we pursued this program by observing NGC 1377 in  $\text{Pa}\beta$ ,  $\text{Br}\gamma$ ,

[FeII] 1.644 and the  $\text{H}_2$  (1-0) S(1) line at  $2.12 \mu\text{m}$ . We chose as a second comparison galaxy NGC 1022, a bright starburst galaxy with a moderately high  $q$  ratio (Sect. 2.3). In view of the raw data, we decided to observe also  $\text{H}_2$  (2-1) S(1) at  $2.25 \mu\text{m}$  and  $\text{H}_2$  (1-0) S(0) at  $2.22 \mu\text{m}$ . The observations and data reduction are described in Appendix A. The spectra are shown in Fig. 9 and the images and velocity maps in Fig. 10. In both NGC 4491 and NGC 1377, the velocity gradient derived from the line centroids is much smaller than the velocity resolution.

#### 4.1.1. NGC 4491

Using the  $\text{Pa}\beta/\text{Br}\gamma$  decrement as an extinction estimator, we obtain  $A(\text{Pa}\beta) = 0.8$  in the central  $2'' \times 2''$  of NGC 4491, and  $A(\text{Pa}\beta) = 2.4$  in the central  $4.83'' \times 4.83''$  of NGC 4102. This is assuming an intrinsic  $\text{Pa}\beta/\text{Br}\gamma$  ratio of 5.58, valid for  $T_e = 5000 \text{ K}$  and  $n_e = 300 \text{ cm}^{-3}$  (Storey & Hummer 1995), and adopting the extinction law of Cardelli et al. (1989). These extinctions are equivalent, in the  $\text{H}\alpha$  line, to respectively 2.4 and 7.3.

Although the absolute central star formation rate of NGC 4491,  $(0.04 \pm 0.02) \text{ M}_\odot \cdot \text{yr}^{-1}$  using the calibration of Kennicutt (1998), is much less than that of NGC 4102,  $(7.6 \pm 0.3) \text{ M}_\odot \cdot \text{yr}^{-1}$ , the  $\text{Pa}\beta$  equivalent widths of the two galaxies are more comparable: we measure respectively  $6.65 \text{ \AA}$  in  $2'' \times 2''$  ( $2.24 \text{ \AA}$  in  $5.7'' \times 5.7''$ ) and  $9.16 \text{ \AA}$ . NGC 4102 is experiencing a powerful outflow (accounting for about one third of the total H recombination line fluxes), at a velocity of  $\approx 800 \text{ km} \cdot \text{s}^{-1}$ , which confirms the youth of its starburst.

The [FeII] 1.644 emission is thought to be due to shock excitation in young supernova remnants (Vanzi & Rieke 1997). As supernovæ appear only a few Myr after the starburst onset, the ratio of the [FeII] line to the hydrogen recombination lines, which are produced almost instantaneously, rises as a function of time elapsed since the beginning of star formation. The [FeII]/ $\text{Br}\gamma$  flux ratio in the center of NGC 4102, corrected for extinction, amounts to about 1.3, which is in the low range of values found in spiral starbursts, between 0.9 and 3 (Moorwood & Oliva 1988). In the central  $2'' \times 2''$  of NGC 4491, [FeII]/ $\text{Br}\gamma$  is constrained to be less than 0.5 at the  $3\sigma$  level. Comparing this to what is expected from the synthesis model of Leitherer et al. (1999) for continuous star formation over a short period, with default parameters (solar metallicity and Salpeter IMF between 1 and  $100 \text{ M}_\odot$ ), the last star formation episode is less than 7.1 Myr old. In the same model, the starburst of NGC 4102 is at least twice older ( $\approx 16.1 \text{ Myr}$ ), but has not reached steady-state either. NGC 4491 is very faint, so our observations are not sensitive enough to produce more stringent a constraint. However, the data are consistent with the idea that NGC 4491 is observed very shortly after the onset of a new episode of star formation, even more recent than in NGC 4102.

For the central  $2'' \times 2''$  of NGC 1022, the galaxy used for comparison with NGC 1377, we derive  $A(\text{H}\alpha) = 4.9$ ,  $EW(\text{Pa}\beta) = 13.88 \text{ \AA}$ , and  $[\text{FeII}]/\text{Br}\gamma \approx 1.6$ . This galaxy has not reached steady-state either, due to its moderately high infrared to radio flux ratio (Section 2.3), and hosts an extranuclear star-formation complex about  $2''$  to the north of the nuclear complex.

#### 4.1.2. NGC 1377

If most ionizing photons are intercepted by dust as suggested by the radio spectrum of NGC 1377, then the hydrogen recombination lines severely underestimate the star formation rate. In agreement with the lack of free-free emission, we detect none of the hydrogen lines. In an area of  $2'' \times 2''$  centered on the nucleus, the  $3\sigma$  upper limits are  $F(\text{Pa}\beta) < 2.24 \times 10^{-19} \text{ W.m}^{-2}$  and  $F(\text{Br}\gamma) < 4.70 \times 10^{-19} \text{ W.m}^{-2}$ .

We do not detect either the shock tracer  $[\text{FeII}]$ , but a strong  $\text{H}_2$  (1-0) S(1) emission line is observed. The  $\text{H}_2$  (2-1) S(1) to  $\text{H}_2$  (1-0) S(1) ratio is less than 0.03 and the  $\text{H}_2$  (1-0) S(0) to  $\text{H}_2$  (1-0) S(1) ratio is less than 0.07, which points to low-velocity shocks as the main mechanism exciting the molecular gas, rather than fluorescence, unless the gas density is high enough to de-excite the molecules by collisions (Hollenbach & Natta 1995) (but the hydrogen nucleus density would have to be higher than  $10^6 \text{ cm}^{-3}$ ). The emission arises in a region smaller than  $2''$ , or 200 pc. In the hypothesis of very high nebular extinction, the  $\text{H}_2$  emission is probably foreground, but it could also originate from the molecular material embedding the newly-formed stars. The young starburst NGC 1022 emits much less flux in  $\text{H}_2$  than in any other line (Table 5) and has a  $\text{H}_2$  (2-1) S(1) to  $\text{H}_2$  (1-0) S(1) ratio of the order of 0.2, so that both shocks and ultraviolet photons can contribute to the molecule excitation.

The lack of hydrogen emission in NGC 1377 may be due partly to lack of ionizing photons and partly to nebular extinction. In the assumption that dust absorbs as much as  $f = 95\%$  of the ionizing photons, as suggested by the lowest radio continuum upper limit (Sect. 3.1), then the dust emission could easily overestimate the star formation rate by a factor of two. With  $SFR_{\text{true}} = SFR_{\text{dust}}/(1 + f)$ , our most stringent limit on the recombination rate still implies a nebular absorption  $A(\text{Pa}\beta) > 3.7$ , or equivalently  $A(\text{H}\alpha) > 11$ . If only 70% of the ionizing photons are absorbed by dust (Sect. 3.1), then  $A(\text{Br}\gamma) > 2.4$ , or  $A(\text{H}\alpha) > 21$ . Either the nebular extinction is very high, or the quasi-totality of the ionizing photons are absorbed by dust, i.e. no HII regions have yet appeared.

To prevent the development of HII regions, massive stars have to still undergo an active accretion-outflow phase, which lasts less than  $10^5$  years (Walmsley 1995). This phase could be responsible for shocking the molecular gas in NGC 1377. Garay et al. (2002) discuss the

properties of a Galactic IRAS source which is a massive star-forming region, still accreting material, and with no free-free emission, hence in a pre-HII region stage. Osorio et al. (1999) modelled the dust emission from an accreting OB star, and obtained spectral energy distributions strikingly similar to the 3–100  $\mu\text{m}$  spectrum of NGC 1377 in its qualitative features. We thus propose that NGC 1377 may host a proto-cluster of this type of object, accounting for an unknown fraction of its infrared luminosity. In this case, a large part of dust heating might not be provided by the direct radiation from massive stars, but by the accretion luminosity (Osorio et al. 1999), and in view of the luminosities computed for a range of model parameters, of the order of  $5 \times 10^4$  O stars would be needed to generate the total infrared luminosity of NGC 1377, i.e. a few times more than for main-sequence stars.

The continuum emission in the PIFS field of view has the same morphology and orientation as the large-scale stellar emission (Fig. 1) and shows no disturbance. The velocity gradient in the  $\text{H}_2(1-0)\text{S}(1)$  line is much less than the velocity resolution, and the continuum emission does not indicate any stellar density cusp. However, the continuum map ratios reveal an emission excess in the Ks band, in the central 1–2'' (slightly elongated parallel to the major axis). The color excesses with respect to the surrounding bluer area,  $\Delta(H_{1.655} - K_{2.142}) \approx 0.5$  and  $\Delta(J_{1.29} - H_{1.655}) \approx 0.2$ , are not compatible with pure extinction ( $A(H_{1.655} - K_{2.142})/A(J_{1.29} - H_{1.655}) = 0.7$  using the extinction law of Cardelli et al. (1989)), but consistent with the presence of hot dust contributing to the Ks-band emission. Assuming that the hot dust contributes only to the Ks-band flux, and not to the J and H fluxes, we find that  $F_\nu(7.7)/F_\nu(\text{K}_{\text{dust}})$ , the flux density ratio of the mid-infrared peak at 7.7  $\mu\text{m}$  to the Ks-band excess, is of the order of 500. As a comparison, Lu et al. (2003) found an average ratio of 150 in a sample of normal star-forming galaxies (see their Figure 6a). The 6–8  $\mu\text{m}$  mid-infrared emission in NGC 1377 is thus abnormally high not only with respect to the far-infrared emission, but also with respect to the hot dust emission in the Ks band, although its (H-K) color excess is more extreme than in all but one of the galaxies studied by Hunt et al. (2002), drawn from the same sample as the galaxies in Lu et al. (2003).

## 4.2. Star formation rate estimates

Table 6 lists the *total* star formation rates based on an extrapolation of far-infrared fluxes to the 8–1000  $\mu\text{m}$  range (Kennicutt 1998), using the observed spectral energy distribution to compute the 8–42  $\mu\text{m}$  flux and the model of Dale et al. (2001) to estimate the contribution from 122 to 1000  $\mu\text{m}$ , as a function of  $F_{60}/F_{100}$ . Star formation rates in the circumnuclear regions can be derived from the spatially-decomposed mid-infrared fluxes, applying the calibration established in Roussel et al. (2001c). IC 1953 and NGC 4491 are depleted in 7  $\mu\text{m}$

emission with respect to the far-infrared, which could mean that the aromatic band carriers are destroyed in these high dust-temperature galaxies; the  $7\ \mu\text{m}$  calibration is therefore not applicable to them without correcting for the grain destruction effect. Considering that galaxies from which the calibration was derived have  $L_7/L_{\text{FIR}}$  ratios between 0.12 and 0.25, and that this quantity is about 0.02 in the center of IC 1953 and 0.04 in NGC 4491, we estimate star formation rates of respectively  $1.65 \pm 0.60\ \text{M}_\odot\text{.yr}^{-1}$  and  $0.3 \pm 0.1\ \text{M}_\odot\text{.yr}^{-1}$ . These numbers are not far below the *total* star formation rates. NGC 1377, on the contrary, has a  $7\ \mu\text{m}$  to far-infrared flux ratio similar to normal and disk-dominated galaxies (Fig. 6). Although the 6–11  $\mu\text{m}$  spectrum of NGC 1377 reveals that the dust responsible for the emission in this range is peculiar, the star formation rate derived from  $F_7$  agrees to within 3% with that derived from the total dust emission for NGC 1377 (Table 6).

To further characterize the star formation activities in the central regions of IC 1953 and NGC 4491, a comparison of their mid-infrared data with those of circumnuclear starbursts and merging galaxies, for which ionizing photon flux densities derived independently are available, can be instructive. Using the circumnuclear regions of the galaxy sample of Roussel et al. (2001a), the starburst galaxies M 82, NGC 253 and NGC 1808, and the merging systems Arp 220 and NGC 6240 to span a range of more than five orders of magnitude in star formation surface density, we found a well-defined relationship between the mid-infrared color and the ionizing photon flux density (Förster-Schreiber & Roussel in preparation).  $7\ \mu\text{m}$  fluxes show no appearance of saturation and remain valid star formation tracers up to ionizing photon flux densities as high as  $5 \times 10^{48}\ \text{s}^{-1}\ \text{pc}^{-2}$ , but decline steadily above that threshold (Förster-Schreiber & Roussel in preparation). The colors of IC 1953 and NGC 4491 suggest that their star formation is more compact than in the M 82 core. If this assumption is correct, this corresponds to ionizing photon flux densities above  $10^{16}\ \text{s}^{-1}\ \text{m}^{-2}$ . Combined with star formation rates derived from the total infrared emission, upper limits on the sizes of the star-forming cores can be inferred: diameters of less than 125 pc and 70 pc are respectively obtained. In the blackbody assumption, we obtain lower limits of 46 pc and 35 pc.

The derived star formation rates are only of the order of  $0.3\text{--}2\ \text{M}_\odot\text{.yr}^{-1}$ . However, the three galaxies have low masses. Comparing these rates with the underlying stellar mass, as traced by the Ks-band light, we find that the timescale to build up an equivalent mass is only of the order of 0.5–2 Gyr in the central  $\approx 5''$  of NGC 1377, IC 1953 and NGC 4491 (using  $M/L_{\text{Ks}} = 0.7\ \text{M}_\odot/L_{\text{Ks}}$ , as found by Grosbol & Patsis (1998), with  $\text{Ks}_\odot = 3.33\ \text{mag}$ , from Colina et al. (1996)). As a comparison, this timescale is similar for the starburst in NGC 4102 (1.7 Gyr) and much longer in the bright star-forming center of the normal spiral NGC 4535 (of the order of 10 Gyr). The star formation activity in the three galaxies can thus be truly identified with starbursts.

Using the star formation rate range derived from dust emission, and comparing it with the extinguished star formation rate derived from the  $H\alpha$  line, we derive an absorption in  $H\alpha$  between 4.3 and 4.9 for the circumnuclear region of IC 1953. If the [NII] to  $H\alpha$  ratio were unusually high such as in NGC 1377, then the nebular absorption could be even higher.

For NGC 4491, we have measured the star formation rate from near-infrared hydrogen recombination lines in the PIFS field of view. The  $7\ \mu\text{m}$ -emitting region may be larger than this, but the strong discrepancy between the recombination estimate and the dust estimate (Table 6) points to either a major fraction of the nebular emission being completely screened, or an overestimation of the star formation rate by the infrared emission, unless photospheric absorption from a young stellar population strongly affects the hydrogen line strengths.

### 4.3. Excitation of the interstellar medium

Far-infrared lines due to collisional excitation in photodissociation regions and ionized regions were observed by ISO-LWS with an effective beam of  $78''$  (LWS handbook). This beam is much larger than the size of the infrared emission of NGC 1377 and NGC 4491, but encompasses only 60% of the total  $7\ \mu\text{m}$  emission of IC 1953. Fluxes are collected in Table 7.

The [CII] 157.7 line is the major coolant of photodissociation regions. Since aromatic band carriers dominating the emission in the  $7\ \mu\text{m}$  bandpass are of planar structure, they are thought to be more efficient sources of photoelectric heating than three-dimensional dust grains (d'Hendecourt & Léger 1987). This finds a confirmation in the constancy of the [CII] to  $7\ \mu\text{m}$  flux ratio found by Helou et al. (2001) in star-forming spiral galaxies. NGC 4491 and IC 1953 behave exactly as this sample: their  $F_{[\text{CII}]} / F_7$  ratios are within  $1.5\sigma$  of the average value. Their  $F_{[\text{CII}]} / F_{\text{CO}}$  ratio is of the order of 2000–4000, depending on the assumed CO spatial distribution, or less, owing to the smaller CO beams in the observations of Boselli et al. (1995) and Combes et al. (1994) (respectively  $33''$  and  $44''$ ). These values are typical of normal star-forming galaxies, and argue for near-solar metallicities, since metal-deficient galaxies will have much higher ratios (Madden 2000). However, NGC 1377 appears deficient in [CII] by at least an order of magnitude and lies more than  $6.5\sigma$  (in dex units) below the average  $F_{[\text{CII}]} / F_7$ . Interestingly, the  $7\ \mu\text{m}$  flux in NGC 1377, which is not produced by classical aromatic particles, is also 0.85 dex higher than expected from its 60 and  $100\ \mu\text{m}$  fluxes (Fig. 5). The species responsible for the  $7\ \mu\text{m}$  emission in NGC 1377 is thus either not easily photoionized, because already highly ionized in its equilibrium state, or is heated mainly by low-energy photons, which is unlikely owing to the observed high dust temperatures in this galaxy, or is not an efficient purveyor of photoelectrons if its structure is not planar.

$C^+$  is collisionally de-excited above relatively low densities, such that the [CII] deficiency of NGC 1377 could be due to increased density; but [OI] 63 remains an efficient cooling agent at densities 100 times higher. Since the  $F_{[OI]}/F_{FIR}$  ratio of NGC 1377 is also low compared to the values it takes in Malhotra et al. (2001), this explanation can be ruled out. Malhotra et al. (2001) also discard high optical depths in  $C^+$  as the cause of the [CII] deficiency (relative to the far-infrared flux) in their high- $F_{60}/F_{100}$  galaxies, because they would expect [OI] to become optically thick before [CII], which they do not observe. A plausible origin of the [CII] deficiency in NGC 1377 is thus a radiation field intense enough to highly ionize the small dust particles emitting in the mid-infrared, which then cannot heat the interstellar medium, and different structural properties of these particles than in normal galaxies. Alternatively, since HII regions seem to be absent in NGC 1377 (Sect. 3.1 and 4.1.2),  $C^+$  ions may not exist and thus be unable to act as a coolant. In any case, the [CII] deficiency is unusual and puzzling.

The upper limits on  $F_{[NII]}$  are within the range of detections at lower dust temperatures of Malhotra et al. (2001), when normalized by the far-infrared flux.

## 5. Molecular gas

NGC 1377 was observed in the CO(1-0) and CO(2-1) lines at the SEST in January 2003, during three sessions of 7 h each, as part of the ESO time share. Important details on the observations can be found in Appendix B. The measurements and results are given in Table 8.

We measure  $\int T_A^* dV = (1.75 \pm 0.12) \text{ K km s}^{-1}$  for the CO(1-0) line and a CO(2-1) to CO(1-0) brightness temperature ratio of  $0.53 \pm 0.14$ . The spectra are shown in Figure 11. The averages of the spectra of the five centermost pointings are shown in Figure 12. The CO(2-1) line profile is perfectly fitted by a gaussian of FWHM  $66 \text{ km s}^{-1}$ ; the CO(1-0) line profile can be fitted by a gaussian of the same width and centered at the same velocity, but shows a wing toward high velocities. This excess is only at the  $2\sigma$  level. For lack of adequate constraints on the  $H_2$  mass to CO luminosity ratio, we adopt a standard value of  $2.3 \times 10^{24} \text{ molecules m}^{-2} (\text{K km s}^{-1})^{-1}$  (Strong et al. 1988), which is uncertain by a factor of at least a few. For infrared-luminous starbursts in which CO is subthermally excited, assuming virialized clouds, Radford et al. (1991) derive factors between about 2 and  $7 \times 10^{24}$ , in the same unit. Due to its low CO(2-1) to CO(1-0) brightness ratio, collisional excitation of the molecular gas in NGC 1377 seems to be also subthermal. Garay et al. (1993) similarly found very low CO(2-1) to CO(1-0) brightness ratios in starburst galaxies, that suggest that most of the emission comes from low-density and very clumpy gas (Park & Hong 1995), while the

star-forming cores are probably hidden by their envelopes. We derive a hydrogen mass of the order of  $2.0 \times 10^8 M_\odot$ . This is at least ten times more than the minimum mass required by the starburst hypothesis (Sect. 3.1). The far-infrared to CO flux ratio is about seven times higher than the average for normal galaxies, but within the broad range observed for starbursts (Sanders & Mirabel 1985), which is not surprising owing to the high dust temperature and emissivity in NGC 1377. The total gas mass to blue luminosity ratio lies at the upper bound of the range measured by Welch & Sage (2003) for a volume-limited sample of lenticular galaxies. The timescale to consume all the molecular gas, including the mass of helium and metals, at the current star formation rate derived from the far-infrared emission, can be estimated to only  $\approx 170$  Myr.

The CO(1-0) line was also observed in IC 1953, NGC 4491 and NGC 4418 (see below a discussion of this galaxy), with smaller signal to noise ratios (Combes et al. 1994; Boselli et al. 1995; Sanders et al. 1991). In all cases, the velocity profile is very narrow (approximate FWHM of 120, 80 and 120  $\text{km s}^{-1}$ ), and the direct effect of rotation invisible, which argues for a concentration of the molecular gas in a small central area. The size of the molecular disk, even if it cannot be directly estimated, can be coarsely constrained by indirect arguments. If one assumes that NGC 1377 must follow the same Schmidt law as characterized by Kennicutt (1998) from normal spirals to starbursts, within the observed scatter, then the diameter of the gas disk should be  $(150 \pm 300)$  pc. Dynamics can be used to set an independent constraint, but one has to make the unverified assumption that the CO disk is coplanar with the stellar disk, which could be false if the gas was accreted from another galaxy. The maximum velocity, corrected for inclination, is about  $90 \text{ km s}^{-1}$ . In case the gas is decoupled from stars (i.e. the stars are distributed in a much more extended structure with a significant plane-perpendicular scale height), the diameter is about 330 pc. If the gas is confined within this region, then it accounts for a large fraction of the total enclosed mass: at least a quarter, estimating the stellar mass from the Ks image.

We now compute the Toomre parameter for local gravitational stability,  $Q_g = v_s \kappa / (\pi G \mu_g)$  (Toomre 1964), in the same manner as usually done for galactic centers, i.e. assuming a gas density  $\mu_g$  equal to the average, and the epicyclic angular velocity  $\kappa = 2V/R$  in the linear part of the rotation curve. The sound speed  $v_s$  is chosen of the order of  $10 \text{ km s}^{-1}$ , and the diameter  $4''$  (400 pc). In these conditions,  $Q_g \simeq 0.3$ , which means that the gas is locally very unstable. We neglected stars, although they influence the gas stability, but they are expected to only decrease it (Jog & Solomon 1984). The parameters entering  $Q_g$  are all ill-constrained, and there is no guarantee that the gas is distributed in a thin disk, but if it is the case, since values close to unity are routinely found in the literature (indicating gravitational stability allowing the mild growth of perturbations), it is at least likely that the molecular gas disk of NGC 1377 be overcritical. This would explain the instantaneous



trigger of a starburst throughout  $\approx 100$  pc. Sound evidence clearly requires more detailed data, difficult to obtain owing to the low brightness of NGC 1377.

Finally, the CO flux can be coupled with the H<sub>2</sub> line measurements described in Section 4.1.2, to estimate the mass fraction of hot molecular gas. The H<sub>2</sub> (1-0) S(0) upper limit does not bring any useful constraint, but the lower limit on the H<sub>2</sub> (1-0) S(1) / H<sub>2</sub> (2-1) S(1) flux ratio implies temperatures below 1500 K. With standard assumptions (due to lack of constraints by the observations), the hot H<sub>2</sub> mass is then above 250 M<sub>⊙</sub>, and the fraction of hot gas is above  $\approx 10^{-6}$ . Such a fraction is in the normal range found for bright starburst galaxies and cannot be further constrained.

## 6. NGC 4418: similarities and differences

NGC 4418, mentioned by Yun et al. (2001) as a high- $q$  galaxy, is an interesting case for which very valuable data exist. Its far-infrared luminosity is  $\approx 5 \times 10^{10} L_{\odot}$ , with  $L_{\text{FIR}}/L_{\text{B}} \approx 35$ ,  $F_{60}/F_{100} = 1.44$  and  $F_{25}/F_{60} = 0.21$ . The NVSS map shows a second source without any optical counterpart about 1.25' to the east, which is certainly included in the IRAS fluxes; depending if this source is included or not in the 21 cm flux, the  $q$  ratio of NGC 4418 is 3.02 or 3.09, between 3.5 and 3.9 $\sigma$  above the average ratio.

Spoon et al. (2001) show that its mid-infrared spectrum presents a broad feature similar to that observed in NGC 1377, but with strong ice absorption bands superposed, which are almost never observed. Other peculiarities of this galaxy are the detection of the H<sub>2</sub> line at 2.12  $\mu\text{m}$  in emission (Ridgway et al. 1994) and of an OH megamaser (Martin et al. 1988). Dudley & Wynn-Williams (1997) suggested that, like in Arp 220, the infrared emission arises from an extremely compact energy source.

NGC 4418 is also deficient in [CII], but  $F_{\text{[CII]}}/F_7$  is only constrained to be more than 2 $\sigma$  below the average ratio in Helou et al. (2001). There are two other major differences with respect to NGC 1377: NGC 4418 has much lower mid-infrared to far-infrared flux ratios, in agreement with the predictions from its high dust temperature, and a very compact radio source is detected at its nucleus, with a brightness temperature of  $10^{4.9}$ – $10^{5.0}$  K both at 2.3 GHz inside 0.1" (Kewley et al. 2000) and at 1.49 GHz inside 0.5"  $\times$  0.3" (Condon et al. 1990). NGC 4418 is not detected in X-rays (Cagnoni et al. 1998). Although the compactness and extreme extinction in NGC 4418 suggest the presence of a Seyfert nucleus, a highly compact starburst is also plausible, and the nuclear 2.2  $\mu\text{m}$  emission is shown to be more extended than the PSF by Eales et al. (1990). The 3.55 cm radio continuum, observed with the VLA in a 0.4"  $\times$  0.25" (J.J. Condon, unpublished) confirms that the radio source is

extended, with a size of  $0.20'' \times 0.16''$ .

During our radio continuum observations of NGC 1377, NGC 4491 and IC 1953 at Efstelsberg, we also mapped NGC 4418 (Fig. 8). We measured  $(33.3 \pm 1.3)$  mJy at 6.2 cm and  $(19.7 \pm 1.2)$  mJy at 3.6 cm (the beam including the source located  $1.25'$  eastward). Combined with the NVSS flux at 21 cm,  $(47.9 \pm 1.8)$  mJy (with the contaminating eastward source added to NGC 4418), this indicates a pronounced spectral bend from a steep index at high frequencies ( $S_{[3-6\text{ cm}]} \propto \nu^{-0.94}$ ) to a flat index at low frequencies ( $S_{[6-21\text{ cm}]} \propto \nu^{-0.30}$ ). The implied high free-free opacity is consistent with the high extinction and compactness of NGC 4418. We find that the combined effect of both thermal opacity and a reduction of the intrinsic synchrotron emission (with respect to the level expected from the far-infrared emission) provides the best fit to the spectrum. The lowest possible opacity and most reasonable non-thermal spectral index,  $\tau(21\text{ cm}) = 0.9$  and  $\alpha_{\text{nth}} = -1.17$ , are obtained for an intrinsic deficit of synchrotron emission of about 50%. Diminishing the synchrotron deficit in the model causes the opacity to rise and the spectral index to become steeper; assuming no deficit,  $\tau(21\text{ cm})$  would have to be as high as 1.6 and  $\alpha_{\text{nth}}$  as low as -1.57.

J.J. Condon obtained with the VLA-A a higher flux at 3.6 cm: 27.4 mJy, including the contaminating eastward source. Using this measurement instead of the single-dish flux, we obtain a maximum opacity  $\tau(21\text{ cm}) = 0.5$ , the steepest possible non-thermal spectral index is  $\alpha_{\text{nth}} = -0.7$ , and in such conditions, the intrinsic synchrotron emission is reduced by 70% with respect to a galaxy with normal  $q$  ratio.

Based on this new result, and on the other existing evidence, we argue that the infrared emission of NGC 4418 originates from a very young and compact starburst. Seyfert activity is not necessary to explain the data. The emission line properties of NGC 4418 are also strikingly similar to those of NGC 1377. It was observed with the PIFS spectrograph by Dale et al. (in preparation), who detected neither Pa $\beta$ , Br $\gamma$  nor [FeII] 1.644, but a clear H<sub>2</sub> (1-0) S(1) line. This fact strengthens the similarity between the two galaxies, and suggests a common excitation mechanism; since NGC 4418 is a synchrotron source, though, it must have reached a later evolutionary stage than NGC 1377, and is possibly a composite source containing both a nascent starburst and a more evolved component.

## 7. Scenarios for the synchrotron deficiency

We now discuss plausible physical scenarios to account for the high infrared to radio ratios of the three galaxies we have studied. If they are due to a deficit of radio emission, then the primary possibility is a lack of cosmic rays, which would follow either from a nascent

starburst or from an initial mass function biased towards low-mass stars; the alternative is a very weak magnetic field. If the radio emission is not depressed, then it might be absorbed, pointing to optically-thick 20 cm emission. Finally, we discuss the possibility of non-stellar activity providing dust heating but remaining radio-quiet.

### 7.1. Nascent starbursts

The hypothesis that we favor to explain the infrared activity and the radio deficiency of NGC 1377, NGC 4491 and IC 1953 is the onset of a star formation burst in their centers. In this view, the synchrotron weakness derives from a lack of relativistic electrons, which can happen if the previous major star formation episode occurred more than  $\approx 10^8$  years ago, and the current episode started less than a few (1 to 7) Myr before the epoch of observation. In NGC 1377 and the central region of IC 1953, no synchrotron component is detected, which implies in this scenario that no or very few supernovæ have yet been produced. In NGC 4491, the synchrotron component does exist but has a much flatter than usual spectral index. We interpret this as due to an energy distribution of cosmic rays inflated with high energies, rather than the effect of free-free opacity; the number of relativistic electrons released by supernovæ is significant, but may still be rising, and the near-infrared spectroscopic results indicate that shocks are weaker than expected from a steady-state situation.

Other observations consistent with this scenario are: the high dust temperatures, indicating starburst-like radiation intensities; the extreme  $F_{15}/F_7$  flux ratios of NGC 4491 and IC 1953, suggesting that very young stellar populations are dominating the dust heating; the mid-infrared spectrum of NGC 1377, which suggests that dust nanoparticles have not been processed into classical aromatic components radiating in normal star-forming galaxies.

### 7.2. Initial mass function

Since the mass spectrum of stars able to heat the dust extends to much lower values than that of stars producing supernovæ, high infrared to radio flux ratios could be achieved if the initial mass function had a very steep slope, making high-mass stars rarer than in normal galaxies. In this hypothesis, the extreme dust temperatures would however require extreme stellar densities. To be compatible with the 21 cm upper limit of NGC 1377, the cutoff of a truncated Salpeter IMF would have to be less than  $8 M_{\odot}$ , since supernovæ have to be totally suppressed. However, according to the model of Désert et al. (1990), the  $F_{60}/F_{100}$  ratio of NGC 1377 implies an average radiation field about 400 times higher than the solar

neighborhood field throughout the dust emission region. Reaching this radiation field with only  $M < 8 M_{\odot}$  stars is impossible to reconcile with the data, as we will show with a simplistic model assuming a uniform stellar distribution. The Ks-band image gives us a constraint on the stellar mass density. The  $H\alpha$ + $[NII]$  map of Heisler & Vader (1995), of better resolution than the infrared maps, delineates a central region of radius  $\approx 5''$ . Using the model of Leitherer et al. (1999), we computed the bolometric power per unit of stellar mass produced by a star formation episode lasting 10 Myr (IMF-truncated) and by an older population of 1 Gyr, as well as their mass to light ratios in the Ks band (close to  $1 M_{\odot}/L_{\odot Ks}$ ), and then the resulting radiation field in the center as a function of the mass fraction of the younger population. Using the value of the solar neighborhood radiation field given by Mathis et al. (1983), we find that the radiation field is high enough only if more than 80% of the mass is locked in the IMF-truncated starburst, hence the mass of any old stellar population is negligible. Since this is unrealistic, an abnormal IMF is unlikely to cause the observed synchrotron deficiency in NGC 1377. In IC 1953, the average radiation field intensity implied by the dust temperature is only 100 times the solar neighborhood value (in fact more than 200 times in the circumnuclear region, according to the decomposition shown in Fig. 5), but the required stellar density is still much higher than that observed, unless more than 65% of the central mass had been generated by a recent starburst.

### 7.3. Magnetic field and inverse Compton losses

The hypothesis of a weak magnetic field remains difficult to rule out. However, if the magnetic energy density of some galaxies happened to be 10–40 times lower than in normal galaxies, it would be difficult to explain why this is so rare and why this deficiency is connected with high dust temperatures, which are observed in all high- $q$  galaxies, unless it is causally linked with the occurrence of a starburst. If the magnetic pressure is unusually low, then cloud collapse is more efficient and a starburst can be triggered at relatively low gas densities; however, the question remains of what caused the low magnetic pressure, and why the starburst was not triggered before. It is also possible, if magnetic fields are usually amplified by a starburst due to increased turbulence, that there is a time delay for the adjustment of the magnetic field; this would become a likely scenario if we detected significant shock excitation by supernovæ by means of the  $[FeII]$  emission line. Note however that the radio spectra of NGC 4491, NGC 4418 and the disk of IC 1953 bring evidence of a normal magnetic field strength, because they show substantial synchrotron emission, and that no signs of supernova shocks exist yet for NGC 1377.

Random magnetic fields of a few  $\mu G$ , about half the typical strength of total magnetic

fields in spiral galaxies, are expected from turbulence alone, even in the absence of large-scale dynamo action. Field strengths of several  $\mu\text{G}$  are easily obtained in elliptical galaxies although they are devoid of rotation (Lesch & Bender 1990; Moss & Shukurov 1996), comparable to strengths in spirals. Unbiased statistical information about synchrotron emission of ellipticals is uneasy to find, but they are much weaker radio emitters than spirals, and their activity is mostly due to Seyfert nuclei (Condon et al. 2002a); their star formation rates are too low to produce enough cosmic rays. Magnetic field amplification by large-scale dynamo processes occurs on timescales as large as  $5 \times 10^8$  years (Beck et al. 1996). However, the growth of random fields requires much less time. Depending on the turbulence characteristics, in particular the cut-off scale, the fastest-growing modes in a predominantly neutral medium may develop on timescales as small as  $10^4$  years, according to Subramanian (1998).

As pointed out by Lisenfeld et al. (1996), the fact that quiescent galaxies and starbursts follow the same infrared-radio correlation, despite the large expected differences in inverse Compton losses, suggests that the total magnetic field grows subsequent to a starburst. If inverse Compton losses are dominant over synchrotron losses, the lifetime of relativistic electrons is inversely proportional to the radiation energy density. Assuming a size of 100 pc for the infrared-emitting region of NGC 1377 (see Sect. 3.1), the radiation energy density integrated between 3 and  $120 \mu\text{m}$ , at the surface of the region, is of the order of  $5 \times 10^{-10} \text{ J m}^{-3}$ . In the ultraluminous compact starbursts studied by Condon et al. (1991b), the typical radiation energy density is estimated to be six times higher than this, and yet they are strong radio continuum emitters, so that synchrotron losses must at least balance inverse Compton losses: mechanisms at work to amplify magnetic fields seem to conspire to produce a constant ratio of magnetic energy density to radiation energy density. This must occur on timescales comparable to or shorter than the growth time of the supernova rate, otherwise significant deviations from the correlation would be observed.

The issue of magnetic field strength is unsettled for NGC 1377, but we would like to stress that a weak field is not required to explain the synchrotron deficiency, since it is easily achieved by lack of cosmic rays, consistent with the fact that no supernova activity is observed. Furthermore, a separate cause has to be sought to explain the absence of free-free emission, which is unaffected by the magnetic field strength.

Alternatively, if the magnetic field in a galaxy were amplified beyond normal values, it would cause more intense radio emission for the same injected population of cosmic rays, since the synchrotron emissivity scales as a large power of the field strength (index between 2 and 4). As a result, the infrared-to-radio ratio would decrease, but the radio emission would fade faster after an episode of star formation. If the magnetic field became so strong that the cosmic rays decayed very fast, the synchrotron emission would appear in intense

bursts followed by periods of radio quiescence. In a steady-state situation, allowing some uncertainty range for the IMF slope, one would expect from the infrared luminosity of NGC 1377 a type-II supernova explosion, on average, at least every 100 years. Thus, cosmic rays should be injected into the interstellar medium, after a time delay, at this average rate. For the lifetime of cosmic-ray electrons to be reduced to 100 years or less at GHz frequencies, a magnetic field of the order of 50 mG would be required over large portions of the interstellar medium (Condon 1992), that is to say  $5 \times 10^3$  times higher than the typical strength in spiral galaxies (Beck 2001). No amplification mechanism is known to achieve such a result on large spatial scales, and such a strong field would clearly not be confined (Parker 1966). Invoking such absurd values of the magnetic field is much less credible than the nascent starburst hypothesis. As a comparison, Carilli & Barthel (1996) estimate fields strengths up to  $350 \mu\text{G}$  in the radio-loud galaxy Cygnus A, using the assumption of minimum energy density for the sum of cosmic rays and magnetic fields. Starburst galaxies may have magnetic fields of a few  $10 \mu\text{G}$ , generally calculated under the same minimum-energy assumption; for instance, Klein et al. (1988) derived an equipartition total field of  $50 \mu\text{G}$  in M 82.

#### 7.4. Electron opacity

We can discard high opacity at 21 cm as the reason for radio weakness, because it would require NGC 1377 and IC 1953 to have respectively  $\tau(21 \text{ cm}) > 2.8$  and  $\tau(21 \text{ cm}) > 0.5$ , only in order to have an intrinsic  $q$  of  $\bar{q} + 2\sigma$ , and NGC 4491 would have to feature an unrealistic geometry. High opacities are very unlikely, since the high- $q$  ultraluminous compact starbursts studied by Condon et al. (1991b) (with  $q > \bar{q} + 3\sigma$ ), much more active and dense, have estimated opacities of only 0.5–0.7.

#### 7.5. Seyfert activity

The infrared-radio properties of NGC 1377 and NGC 4491 may be suggestive of the presence of active nuclei in these galaxies. However, spectral diagnostics do not support this view, since emission lines are either absent or very weak and narrow.

Two indirect arguments can be put forward to support the presence of a Seyfert nucleus: warm infrared colors, and the compactness of the infrared emission. We consider the argument of deep silicate absorption in the 9–11  $\mu\text{m}$  range in NGC 1377 speculative, especially since the continuum emission longward of 11  $\mu\text{m}$  has not been observed, and because it would be difficult to reconcile with the moderate dust to stellar emission power ratio; diagnostics

based on optical spectroscopy cannot be applied. However, the above two characteristics support equally well the hypothesis of a young starburst. The mid-infrared spectrum is an extremely ambiguous diagnostic, since it does not show the aromatic bands associated with star formation, but does show an unusual emission feature, in place of the continuum expected in a pure Seyfert nucleus. Concerning the infrared broadband colors, Yun et al. (2001), for instance, have shown that they are not valid discriminants between starburst and Seyfert activities – even if a larger percentage of energetically-dominating Seyfert galaxies is found in any sample pre-selected to have warm colors, than in a sample with cooler colors. The concentration factor is not a strong argument either, since a young starburst will be compact (to trigger a star formation burst instantaneously over a large area requires uncommon conditions); the data for NGC 1377 suggest that the size could be as small as  $\approx 100$  pc, i.e.  $1''$  (Sect. 3.1), and is smaller than  $\approx 2''$ , i.e. 200 pc (Sect. 4.1.2). In addition, Seyfert nuclei powerful enough to dominate dust heating tend to occur in massive galaxies with a deep potential well, whereas NGC 1377 is a low-mass galaxy and with a shallow potential. But perhaps the most problematic fact for Seyfert activity is the radio deficiency.

Many active nuclei are known to be radio-quiet. However, their  $q$  ratios are the same as in normal galaxies. For instance, the infrared-loud and radio-quiet quasar studied by Beichman et al. (1986) has an observed  $q = 2.48 = \bar{q} + 0.75\sigma$ , even if it is strongly absorbed at 20 cm. In the sample of Ho (2002), containing a large number of radio-quiet active nuclei, no nucleus has a  $q$  ratio significantly higher than the average for normal galaxies; all the Seyfert-type galaxies which are not detected at 20 cm are not detected by IRAS either. We have further verified this fact by selecting in the NED database all galaxies in the quasar category with  $F_{60} > 0.5$  Jy and no mention of a radio association; on the 53 objects thus selected, 7 were excluded for lack of any radio observations, and all the others have either normal or low  $q$  ratios. The infrared brightness of NGC 1377 thus presents serious difficulties for the hypothesis of a radio-quiet active nucleus.

An examination of the energetics provides another argument against the production of the infrared power of NGC 1377 by an active nucleus. Assuming that the radiated power is equal to the Eddington limit,  $L_E(W) = 1.3 \times 10^{31} M_{\text{BH}} (M_{\odot})$ , and that it goes entirely into dust heating, an upper limit on the black hole mass provides an upper limit on the infrared power. For a given black hole mass, the radio loudness can vary considerably (e.g. Woo & Urry (2002)); but for radio-quiet active nuclei exclusively, estimating black hole masses from reverberation mapping techniques, Nelson (2000) found a correlation between the black hole mass and the radio power, with a lower envelope of all their data of the form  $P(20 \text{ cm})(W \text{ Hz}^{-1}) = 10^{15.2} (M_{\text{BH}}/M_{\odot})^{0.84}$ . Using the 20 cm upper limit for NGC 1377, the alleged black hole cannot be more massive than  $2.4 \times 10^5 M_{\odot}$ . Using alternatively the kinematic information derived from the  $\text{H}_2$  emission line (Sect. 4.1.2), another limit can be

set. With a velocity gradient below  $40 \text{ km s}^{-1}$ , the inclination-corrected rotation velocity is less than  $25 \text{ km s}^{-1}$  (with a signal to noise ratio of  $\approx 5$  throughout the central  $2''$ ). Assuming virial equilibrium, and provided the  $\text{H}_2$  lies in the plane of the galactic disk, we then do not expect more than  $1.5 \times 10^5 M_\odot$  to be enclosed in the central parsec. Using the first upper limit, we thus find that the maximum infrared power (in extremely unrealistic conditions) radiated by an active nucleus is  $3 \times 10^{36} \text{ W}$ . In fact, it is expected to be a factor of several below this value, because the dust heating efficiency cannot be 100%. The infrared luminosity of NGC 1377 being  $3.9 \times 10^{36} \text{ W}$ , an active nucleus cannot easily account for it.

The absence of synchrotron emission might be attributed to lack of magnetic field (Sect. 7.3), or extreme inverse Compton losses, due to the high radiation field intensity in NGC 1377. Nevertheless, an active nucleus must also produce some free-free emission, which is not detected either. Inside the region where dust grains are sublimated, the Lyman continuum photons are free to ionize the gas, contrary to the situation in an embedded starburst. Elvis et al. (1994) have compiled spectral energy distributions of quasars and estimated, in particular, the ionizing photon flux and the total power between  $1000 \text{ \AA}$  and  $100 \mu\text{m}$ . The ratio between these two quantities is  $N_{\text{ion}}/L_{UV-IR} = (8.1 \pm 2.9) \times 10^{16} \text{ s}^{-1} \text{ W}^{-1}$  (or  $L_{\text{ion}}/L_{UV-IR} = 0.5 \pm 0.2$ ). Taking the infrared luminosity of NGC 1377 as a lower limit to  $L_{UV-IR}$  and assuming that the ionizing photon flux available in the dust-free region is equal to  $N_{\text{ion}}/2$ , the free-free emission at  $3.6 \text{ cm}$ , where thermal opacity is negligible, should amount to  $\approx (2.8 \pm 1.0) \text{ mJy}$  (with  $T_e = 5000 \text{ K}$ ). It would thus have been detected, especially by the sensitive observation with the VLA in the A configuration. The single-dish upper limit is  $2 \text{ mJy}$ , and the VLA upper limit is  $0.13 \text{ mJy}$ . Although we cannot rule out completely the presence of an active nucleus, because the properties of NGC 1377 remain challenging, the above arguments rather support our hypothesis of a nascent starburst.

The properties of NGC 4491 may in turn be indicative of non-stellar activity, because some active nuclei are known to have flat radio spectra. Dust heating by an active nucleus is however very unlikely, owing to the following facts: NGC 4491 has no bulge; the velocity gradient inferred from the  $\text{Pa}\beta$  line (see Section 4.1) is much less than  $100 \text{ km s}^{-1}$ , which confirms that there is no central gravitational cusp (the inclination on the line of sight is about  $62^\circ$ ); optical and near-infrared emission lines do not give any indication of an active nucleus; the dust spectral energy distribution is fully consistent with the properties of star-forming galaxies, whereas one would expect a high mid-infrared to far-infrared power ratio if dust were heated by an active nucleus.



## 8. Frequency of occurrence

Other high- $q$  galaxies, deviating by more than  $3\sigma$  from the average infrared to radio flux ratio, are known, though NGC 1377 is the most extreme case. Among the sample studied by Vader et al. (1993) in a series of papers, comprised of galaxies whose flux density is higher at  $60\ \mu\text{m}$  than at  $100\ \mu\text{m}$ , 31 lie in the NVSS sky coverage (including NGC 1377); of these 31, we find that five galaxies satisfy the above high- $q$  criterion.

Of the 40 very luminous galaxies belonging to the IRAS bright galaxy sample ( $F_{60} > 5.24\ \text{Jy}$  and  $\log(L_{\text{FIR}}/L_{\odot}) > 11.25$ ), Condon et al. (1991b) have found three more high- $q$  galaxies, which are distant (200 to 300 Mpc) and whose flux densities peak at  $60\ \mu\text{m}$ ; they classify them as compact starbursts. The activity of two of them is obviously driven by on-going mergers, with double nuclei separated by less than  $5''$  (Scoville et al. 2000), and the third galaxy presents a strong warp (Lehnert & Heckman 1995). However, Condon et al. (1991b) claim that their radio deficiency is best explained by high free-free opacity at 20 cm, rather than a lack of cosmic rays.

Nine galaxies with  $q > 3$  are mentioned by Yun et al. (2001) in a complete sample of 1809 galaxies with  $F_{60} > 2\ \text{Jy}$  (i.e. with an occurrence rate of 0.5%), two of which in common with Condon et al. (1991b). However, reexamining these galaxies, we find that five of them are false high- $q$  detections, due partly to confusion affecting IRAS fluxes, and partly to NVSS catalog fluxes missing low-surface brightness or extended structures. On the other hand, Yun et al. (2001) have missed NGC 1377, NGC 4491 and two galaxies of the sample of Vader et al. (1993), which, according to the selection criteria of Yun et al. (2001), must be part of their sample and have  $q > 3$ . Because of inevitable errors due to automatic handling of very large samples, the census of high- $q$  galaxies they provide is therefore uncertain. The two new high- $q$  galaxies that they found have  $F_{60}/F_{100}$  ratios of  $\approx 0.9$  and 1.44.

In view of the above numbers, it seems that the most efficient way of finding synchrotron-deficient galaxies is to select high dust temperatures ( $F_{60}/F_{100} \geq 0.8$  for all known high- $q$  galaxies), and that the infrared luminosity matters much less. The occurrence rate in the color-selected sample of Vader et al. (1993) is as high as 16%.  $60\ \mu\text{m}$ -peakers being scarce objects, however, the implied probability for a random local galaxy to be synchrotron-deficient must be very low. The flux-limited sample of Condon et al. (1990) and Condon et al. (1996) (500 galaxies with  $F_{60} > 5.24\ \text{Jy}$ ) contains at least 6 high- $q$  galaxies identified in the above various samples, which implies a rate of the order of 1%.

The incidence of high dust temperatures is an additional argument in favor of the nascent starburst hypothesis that we have developed for NGC 1377, IC 1953 and NGC 4491. In this scenario, the scarcity of high- $q$  galaxies derives naturally from the timescales involved.

The likelihood for a galaxy to have a high  $q$  ratio is the product of the probabilities of two occurrences: it has to have been quiescent for at least  $10^8$  years, and a starburst has to have started less than 3–4 Myr before the epoch of observation. Less than  $\approx 15\%$  of optically-selected galaxies have infrared color excesses indicative of on-going intense star formation, as apparent from the analysis of Huang et al. (1996) (of their “HP sample”); from this we may infer that galaxies spend, on average, less than 15% of the time in starburst events. Given a typical starburst duration of  $f \times 4$  Myr, with  $f \geq 1$ , the second probability listed above is necessarily lower than  $0.15/f$ . While the probability of the first occurrence (quiescence for  $10^8$  years) is difficult to assess, it is sufficiently unlikely that high- $q$  systems should be rare, consistent with the statistics. However, at high redshifts, before the epoch of maximum star formation density, the probability of observing radio-deficient galaxies may be higher. It is unknown beyond what redshift metallicity effects, reducing the amount of dust and thus of infrared emission, will start to compete with the nascent starburst effect. Garrett (2002) recently estimated  $q$  ratios of distant galaxies ( $z$  up to 1.3) and found no significant deviation of the average from the local value.

### 8.1. Triggering mechanisms

The data shown in this paper are consistent with the high infrared to radio flux ratios being caused by a delay in either the magnetic field strength or the cosmic ray density, in either case a consequence of a nascent starburst.

In contrast to the above infrared-luminous galaxies, NGC 1377, NGC 4491 and IC 1953 have a shallow potential well, such that the triggering mechanism of a central starburst is not obvious. In IC 1953, tidal interaction, likely at work, could be responsible for strengthening the bar perturbation (which seems unusually strong for the morphological type of IC 1953) and causing massive gas inflow due to the bar potential. In this view, we would be witnessing the first burst caused by the bar, and IC 1953 will likely have an earlier-type aspect afterwards. NGC 4491 is also strongly barred, and this bar may also have grown due to tidal forces with other Virgo galaxies. However, no evidence of a bar nor of an intrusion exists in the most extreme galaxy of the three, NGC 1377. Are tidal interactions experienced by galaxies in clusters and groups efficient at producing gas inflows inside them, even in the absence of any visible potential perturbation? Other HI-deficient and non-Seyfert Virgo galaxies, besides NGC 4491, indeed have surprisingly high mid-infrared colors in their centers: N4293, N4569, N4579 (Roussel et al. 2001b). Note that all these galaxies either lie close to M 87 in projection and have radial velocities more than  $600 \text{ km s}^{-1}$  away from the velocity centroid (Cayatte et al. 1990), or lie at the periphery of the cluster in projection, which could

mean that they are part of a very turbulent subsystem. Helou et al. (1989) found such an environmental effect in the Virgo unrelaxed subsystem called W, where blue compact dwarf galaxies are more numerous and have hotter dust than in the rest of the cluster.

Hidden perturbations are best revealed by observing the HI morphology and velocity structure, but NGC 1377 seems to have too little HI gas for such a diagnostic to be applied. An assessment of the nature and cause of the activity seen in the three galaxies will have to wait for complementary data.

## 9. Summary and final remarks

In order to understand the cause of the synchrotron deficiency observed in the three closest high- $q$  galaxies, we have presented and analysed extensive data in several windows: broadband dust emission, radio continuum at several frequencies, emission line diagnostics of photon ionization, supernova shocks and hot molecular gas excitation, and emission of the cold molecular gas.

We argued that the galaxies are seen at the very onset of a starburst episode, following a long period of quiescence, based on these data, and consistent with the statistics of high- $q$  galaxies inferred from starburst timescales. In this scenario, cosmic rays generated by past star formation had the time to decay, and massive stars produced by the current star formation episode have not evolved into supernovæ yet (NGC 1377, central region of IC 1953) or, in the case of NGC 4491, the supernova rate is still rising and the cosmic ray population is in its formative stages.

All three galaxies host unusually hot dust, requiring an intense radiation field consistent with that produced by a young starburst. NGC 1377, whose properties are the most peculiar, is not only devoid of synchrotron radiation, but also of free-free emission. We propose that the starburst is so young that massive stars are still accreting material, preventing the development of HII regions. Along the same line, dust emission in the mid-infrared has an unusual spectral signature, suggesting that grains were processed differently from grains found in almost every other star formation environment; the molecular gas disk may be overcritical, which would explain the quasi-instantaneous trigger of a starburst. While this is the most likely explanation, the properties of NGC 1377 remain very intriguing.

We can rule out abnormal initial mass function, electron opacity and fast synchrotron losses as causes of the depressed radio continuum. Other scenarios are not formally ruled out, but create serious difficulties: radio-quiet Seyfert activity is unlikely owing to the energetics arguments discussed in Section 7.5; a weak magnetic field (relevant only for NGC 1377) is

possible, but difficult to explain in light of what is known of turbulent field amplification, and still requires a young starburst after a period of quiescence.

We would like to stress that the galaxies studied in this paper are not akin to irregular or blue compact dwarf galaxies, which would at first sight be easily susceptible of synchrotron deficiency for various reasons: fast cosmic ray escape and interstellar medium disruption and loss; evidence of optically-thick free-free emission in some of them. Although these galaxies seem to have much more dispersed infrared to radio flux ratios than spirals, they follow the same average relationship and none of them is known to deviate from it significantly.

Among galaxies of the IRAS bright galaxy sample, selected by their  $60\mu\text{m}$  flux, the occurrence rate of high- $q$  galaxies (in our interpretation nascent starbursts) is of the order of 1% or slightly more. The best way to select these galaxies is to search for high dust temperatures; no other simple criterion is evident. Although very few examples are known, from this phenomenon arises a potential problem for the identification of distant infrared galaxies with high-resolution radio observations, especially with possibly changing star formation timescales at high redshifts.

The galaxies studied here offer a unique glimpse at starbursts during a critical period of their evolution, and will allow us to address questions concerning the pre-starburst accumulation of molecular material, the triggering mechanisms, the spatial development of a starburst, and the start, build-up and evolution of a cosmic ray population.

We are grateful to Antonio García-Barreto for providing us his ( $\text{H}\alpha + [\text{NII}]$ ) and I-band maps of IC 1953, to Sangeeta Malhotra for mentioning the peculiar infrared properties of NGC 4418, thereby arousing our curiosity, to the persons who assisted us in the observations at Effelsberg, Palomar and La Silla, and to James Brauher for communicating us some fluxes in advance of publication. This publication makes use of data products from the Two Micron All Sky Survey, which is a joint project of the University of Massachusetts and IPAC/Caltech, funded by NASA and the National Science Foundation. The ISOCAM data presented in this paper were analyzed using and adapting the CIA package, a joint development by the ESA Astrophysics Division and the ISOCAM Consortium. This research also benefited from the NASA/IPAC Extragalactic Database (NED), which is operated by the Jet Propulsion Laboratory of Caltech.

### A. PIFS observations

In February, exposures times were 300 s for all lines but [FeII] in NGC 4491, for which it was increased to 400 s. Except for the beginning of Feb. 1, the sky was very clear, and the observations were photometric. Star number 9148 in Persson et al. (1998) was used as a photometric standard. In October, exposure times for NGC 1377 and NGC 1022 were respectively 260 and 220 s for all lines; the flux calibration was performed with 2MASS images.

The field of view of PIFS is sliced into eight slits, 0.67"-wide and 9.7"-long. We dithered to reconstruct cross-slit spatial information, and obtained maps of  $5.8'' \times 10''$ , with a pixel size of 0.167". The high-resolution grating yields resolutions between 950 and 1500 at the wavelengths of interest.

Observations were carried out as outlined in the PIFS manual (which can be found in <http://www.its.caltech.edu/~btsoifer/pifs/>). The flat-field and atmospheric transmission function was calibrated by sweeping G0V–G8V stars across the array with the chopping secondary, using a fast triangle wave, at the same airmass as the galaxy to within 10%. The same stars were chopped in the cross-slit direction in order to establish a flux reference and to calibrate spatial curvature. Noble gas spectra served to correct for spectral distortion and fit the wavelength function. The data reduction consists of the following steps: (1) define a mask for bad pixels and cosmic rays; (2) subtract the bias for each quadrant of the array; (3) subtract the sky, tying the OH line intensities in the off-source spectra to their intensities in the on-source spectra (in the edges of the field, where the contribution from the galaxy is minimal); (4) divide spectra by the flat-field and atmospheric function; (5) construct a wavelength map using the noble gas spectra; (6) correct for the spectral and spatial distortions, and combine the rectified spectra in a cube. Table 5 offers a summary of observing parameters and measured fluxes. In order to minimize residuals from OH sky lines in the faint spectra of NGC 4491, we subtracted the spectral variations of an off-center region around its average flux density.

### B. SEST observations

We used dual beam switching, and connected the IRAM 115/230 receivers to the low-resolution acousto-optical spectrometers. The initial velocity resolution was  $3.6 \text{ km s}^{-1}$  and  $1.8 \text{ km s}^{-1}$ , respectively. System temperatures ranged between 200 K and 400 K at 230 GHz and between 230 K and 460 K at 115 GHz. The beam width is 45" at 115 GHz and 23" at 230 GHz. Baseline fitting and removal in each separate spectrum, and averaging of spectra

obtained at the same position were performed with the CLASS software, which is developed by the Observatoire de Grenoble and IRAM. We used main beam efficiencies of 0.7 at 115 GHz and 0.5 at 230 GHz, and a forward efficiency of 0.9.

Pointing corrections were determined on the closest bright SiO masers,  $\rho$  Ceti and Orion SiO, twice per observing session, at the beginning and after sunset. These sources are respectively about  $15^\circ$  and  $30^\circ$  away from NGC 1377 in azimuth, and about  $15^\circ$  away to the north. Due to these large distances, the pointing accuracy is likely degraded with respect to the quoted value of  $3''$  rms in azimuth and elevation. Furthermore, a hardware limit obliged us to rotate the antenna by  $360^\circ$  in azimuth once per night; because the CO(2-1) spectrum obtained on the center of NGC 1377 before the rotation was not reproduced within the error bar after the rotation, we suspect that this introduced additional pointing errors, and we discarded the redundant data obtained after rotating the antenna.

In order to know whether the CO source is extended, we performed minimal mapping, integrating on the galaxy center and eight adjacent positions stepped by half the CO(2-1) beam width. The spectra are shown in Figure 11. The resulting eighteen total flux measurements were least-squares-fitted with a gaussian source of adjustable width, allowing for some random pointing errors of up to  $3''$  at each position, plus some systematic larger pointing errors after each large rotation of the antenna. If no systematic errors are allowed, then the fit is not acceptable (normalized  $\chi^2 > 8$ ). We can reproduce the data provided these systematic pointing errors are of the order of  $5''$  or slightly more. The best fit is then always obtained for the smallest source size of the explored grid. Due to the large beams, this parameter is not well constrained, but the derived total fluxes are robust results.

## REFERENCES

- Barnes D.G., Staveley-Smith L., de Blok W.J. et al., 2001, MNRAS 322, 486
- Beck R., 2001, SSRv 99, 243
- Beck R., Brandenburg A., Moss D., Shukurov A. & Sokoloff D., 1996, ARA&A 34, 155
- Beck R. & Golla G., 1988, A&A 191, L9
- Beck S.C., Turner J.L. & Kovo O., 2000, AJ 120, 244
- Beichman C.A., Soifer B.T., Helou G. et al., 1986, ApJ 308, L1
- Bianchi S., Davies J.I. & Alton P.B., 1999, A&A 344, L1

- Bicay M.D. & Helou G., 1990, ApJ 362, 59
- Binggeli B. & Cameron L.M., 1993, A&AS 98, 297
- Binggeli B., Popescu C.C. & Tammann G.A., 1993, A&AS 98, 275
- Boselli A., Casoli F. & Lequeux J., 1995, A&AS 110, 521
- Brauher J., 2002, in preparation
- Burrows D.N., Singh K.P., Nousek J.A., Garmire G.P. & Good J., 1993, ApJ 406, 97
- Cagnoni I., della Ceca R. & Maccacaro T., 1998, ApJ 493, 54
- Cardelli J.A., Clayton G.C. & Mathis J.S., 1989, ApJ 345, 245
- Carilli C.L. & Barthel P.D., 1996, A&ARv 7, 1
- Cayatte V., van Gorkom J.H., Balkowski C. & Kotanyi C., 1990, AJ 100, 604
- Chapman S.C., Helou G., Lewis G.F. & Dale D.A., 2002, submitted to ApJ
- Clark D.H. & Caswell J.L., 1976, MNRAS 174, 267
- Colina L., Bohlin R.C. & Castelli F., 1996, AJ 112, 307
- Combes F., Prugniel P., Rampazzo R. & Sulentic J.W., 1994, A&A 281, 725
- Condon J.J., Cotton W.D. & Broderick J.J., 2002a, AJ 124, 675
- Condon J.J., Helou G. & Jarrett T.H., 2002b, AJ 123, 1881
- Condon J.J., Cotton W.D., Greisen E.W. et al., 1998, AJ 115, 1693
- Condon J.J. Helou G., Sanders D.B. & Soifer B.T., 1996, ApJS 103, 81
- Condon J.J., Helou G., Sanders D.B. & Soifer B.T., 1993, AJ 105, 1730
- Condon J.J., 1992, ARA&A 30, 575
- Condon J.J., Huang Z.P., Yin Q.F. & Thuan T.X., 1991, ApJ 378, 65
- Condon J.J., Anderson M.L. & Helou G., 1991, ApJ 376, 95
- Condon J.J. Helou G., Sanders D.B. & Soifer B.T., 1990, ApJS 73, 359
- Condon J.J. & Yin Q.F., 1990, ApJ 357, 97

- Contursi A., Lequeux J., Cesarsky D. et al., 2000, *A&A* 362, 310
- Dale D.A., Roussel H., Contursi A. et al., in preparation
- Dale D.A., Helou G., Contursi A., Silbermann N.A. & Kolhatkar S., 2001, *ApJ* 549, 215
- Désert F.X., Boulanger F. & Puget J.L., 1990, *A&A* 237, 215
- Devereux N.A. & Eales S.A., 1989, *ApJ* 340, 708
- Draine B.T. & Lee H.M., 1984, *ApJ* 285, 89
- Draine B.T., 1981, *ApJ* 245, 880
- Dressel L.L. & Condon J.J., 1978, *ApJS* 36, 53
- Dröge W., Lerche I. & Schlickeiser R., 1987, *A&A* 178, 252
- Dudley C.C. & Wynn-Williams C.G., 1997, *ApJ* 488, 720
- Dwek E., Foster S.M. & Vancura O., 1996, *ApJ* 457, 244
- Eales S.A., Becklin E.E., Hodapp K.W., Simons D.A. & Wynn-Williams C.G., 1990, *ApJ* 365, 478
- Elvis M., Wilkes B.J., McDowell J.C. et al., 1994, *ApJS* 95, 1
- Emerson D.T. & Gräve R., 1988, *A&A* 190, 353
- Engelmann J.J., Ferrando P., Soutoul A. et al., 1990, *A&A* 233, 96
- Fermi E., 1954, *ApJ* 119, 1
- Fomalont E.B., Kellermann K.I., Partridge R.B., Windhorst R.A. & Richards E.A., 2002, *AJ* 123, 2402
- Förster-Schreiber N.M. & Roussel H., in preparation
- Gabel J.R. & Bruhweiler F.C., 2002, *AJ* 124, 737
- Garay G., Brooks K.J., Mardones D., Norris R.P. & Burton M.G., 2002, *ApJ* 579, 678
- Garay G., Mardones D. & Mirabel I.F., 1993, *A&A* 277, 405
- García-Barreto J.A., Franco J., Carrillo R., Venegas S. & Escalante-Ramírez B., 1996, *RevMexAA* 32, 89



- Garrett M.A., 2002, A&A 384, L19
- Genzel R., Lutz D., Sturm E. et al., 1998, ApJ 498, 579
- Giovanelli R., Haynes M.P., Herter T. et al., 1997, AJ 113, 22
- Gordon S.M., Duric N., Kirshner R.P., Goss W.M. & Viallefond F., 1999, ApJS 120, 247
- de Grijp M.H., Miley G.K. & Lub J., 1987, A&AS 70, 95
- Grosbol P.J. & Patsis P.A., 1998, A&A 336, 840
- Guiderdoni B. & Rocca-Volmerange B., 1985, A&A 151, 108
- Guillois O., Nenner I., Papoular R. & Reynaud C., 1996, ApJ 464, 810
- Heisler C.A., de Robertis M.M. & Nadeau D., 1996, MNRAS 280, 579
- Heisler C.A. & Vader J.P., 1995, AJ 110, 87
- Heisler C.A. & Vader J.P., 1994, AJ 107, 35
- Helou G., Malhotra S., Hollenbach D.J. et al., 2001, ApJ 548, L73
- Helou G., Lu N.Y., Werner M.W., Malhotra S & Silbermann N, 2000, ApJ 532, L21
- Helou G. & Bica M.D., 1993, ApJ 415, 93
- Helou G., Hoffman G.L. & Salpeter E.E., 1989, in *The world of galaxies*, Workshop held April 1988 in Paris, ed. Corwin & Bottinelli, p. 496
- Helou G., Khan I.R., Malek L. & Boehmer L., 1988, ApJS 68, 151
- Helou G., 1986, ApJ 311, L33
- Helou G., Soifer B.T. & Rowan-Robinson M., 1985, ApJ 298, L7
- d'Hendecourt L.B. & Léger A., 1987, A&A 180, L9
- Ho L.C., 2002, ApJ 564, 12
- Hollenbach D. & Natta A., 1995, ApJ 455, 133
- Huang J.H., Gu Q.S., Su H.J., Hawarden T.G., Liao X.H. & Wu G.X., 1996, A&A 313, 13
- Hummel E. & Beck R., 1995, A&A 303, 691

- Hummel E., Davies R.D., Wolstencroft R.D., van der Hulst J.M. & Pedlar A., 1988, *A&A* 199, 91
- Hunt L.K., Giovanardi C. & Helou G., 2002, *A&A* 394, 873
- Hunter, D.A., Kaufman M., Hollenbach D.J. et al., 2001, *ApJ* 553, 121
- Jarrett T.H., Chester T., Cutri R., Schneider S. & Huchra J., 2003, "The 2MASS Large Galaxy Atlas", *AJ*, in press
- Jarrett T.H., 2000, *PASP*, 112, 1008
- Jog C.J. & Solomon P.M., 1984, *ApJ* 276, 114
- Jogee S. & Kenney J.D.P., 1995, *BAAS* 27, 1356
- de Jong T., Klein U., Wielebinski R. & Wunderlich E., 1985, *A&A* 147, L6
- Kennicutt R.C., 1998, *ARA&A* 36, 189
- Kewley L.J., Heisler C.A., Dopita M.A. et al., 2000, *ApJ* 530, 704
- Kim D.C., Sanders D.B., Veilleux S., Mazzrella J.M. & Soifer B.T., 1995, *ApJS* 98, 129
- Klaas U., Haas M., Müller S.A. et al., 2001, *A&A* 379, 823
- Klein U., Weiland H. & Brinks E., 1991, *A&A* 246, 323
- Klein U., Wielebinski R. & Morsi H.W., 1988, *A&A* 190, 41
- Kobulnicky H.A. & Johnson K.E., 1999, *ApJ* 527, 154
- Kodaira K., Watanabe M. & Okamura S., 1986, *ApJS* 62, 703
- Koopmann R.A., Kenney J.D. & Young J., 2001, *ApJS* 135, 125
- Kwok S., Volk K. & Bernath P., 2001, *ApJ* 554, L87
- Laureijs R.J., Watson D., Metcalfe L. et al., 2000, *A&A* 359, 900
- Laurent O., Mirabel I.F., Charmandaris V. et al., 2000, *A&A* 359, 887
- Leech K.J., Völk H.J., Heinrichsen I. et al., 1999, *MNRAS* 310, 317
- Lehnert M.D. & Heckman T.M., 1995, *ApJS* 97, 89
- Leitherer C., Schaerer D., Goldader J.D. et al., 1999, *ApJS* 123, 3

- Lesch H. & Bender R., 1990, A&A 233, 417
- Lisenfeld U., Völk H.J. & Xu C., 1996, A&A 314, 745
- Lu N., Helou G., Werner M.W. et al., 2003, ApJ 588, 199
- Madden S.C., 2000, New Astr. Review 44, 249
- Malhotra S., Kaufman M.J., Hollenbach D. et al., 2001, ApJ 561, 766
- Marsh K.A. & Helou G., 1995, ApJ 445, 599
- Martin J.M., Bottinelli L., Dennefeld M., Gouguenheim L. & Le Squeren A.M., 1988, A&A 201, L13
- Mathis J.S., Mezger P.G. & Panagia N., 1983, A&A 128, 212
- Menon T.K., 1991, ApJ 372, 419
- Miller N.A. & Owen F.N., 2001, AJ 121, 1903
- Moorwood A.F. & Oliva E., 1988, A&A 203, 278
- Moss D. & Shukurov A., 1996, MNRAS 279, 229
- Murphy T.W., Matthews K. & Soifer B.T., 1999, PASP 111, 1176
- Nelson C.H., 2000, ApJ 544, L91
- Niklas S., Klein U. & Wielebinski R., 1997, A&A 322, 19
- Niklas S. & Beck R., 1997, A&A 320, 54
- Niklas S., Klein U. & Wielebinski R., 1995, A&A 293, 56
- Osorio M., Lizano S. & d’Alessio P., 1999, ApJ 525, 808
- Park Y.S. & Hong S.S. 1995, A&A 300, 890
- Parker E.N., 1966, ApJ 145, 811
- Pelletier G. & Roland J., 1988, A&A 196, 71
- Persson S.E., Murphy D.C., Krzeminski W., Roth M. & Rieke M.J., 1998, AJ 116, 2475
- Radford S.J., Solomon P.M. & Downes D., 1991, ApJ 368, L15

- Ridgway S.E., Wynn-Williams C.G. & Becklin E.E., 1994, ApJ 428, 609
- Rigopoulou D., Spoon H.W.W., Genzel R., Lutz D., Moorwood A.F.M. & Tran Q.D., 1999, AJ 118, 2625
- Roussel H., Sauvage M., Vigroux L. & Bosma A., 2001c, A&A 372, 427
- Roussel H., Sauvage M., Vigroux L., Bosma A. et al., 2001b, A&A 372, 406
- Roussel H., Vigroux L., Bosma A., Sauvage M. et al., 2001a, A&A 369, 473
- Roy A.L., Norris R.P., Kesteven M.J., Troup E.R. & Reynolds J.E., 1998, MNRAS 301, 1019
- Sanders D.B., Scoville N.Z. & Soifer B.T., 1991, ApJ 370, 158
- Sanders D.B. & Mirabel I.F., 1985, ApJ 298, L31
- Scoville N.Z., Evans A.S., Thompson R. et al., 2000, AJ 119, 991
- Sodroski T.J., Bennett C., Boggess N. et al., 1994, ApJ 428, 638
- Sopp H.M. & Alexander P., 1991, MNRAS 251, SC 14
- Spoon H.W., Keane J.V., Tielens A.G., Lutz D. & Moorwood A.F., 2001, A&A 365, L353
- Storey P.J. & Hummer D.G., 1995, MNRAS 272, 41
- Strong A.W., Bloemen J.B., Dame T.M. et al., 1988, A&A 207, 1
- Strong A.W., 1977, MNRAS 181, 311
- Subramanian K., 1998, MNRAS 294, 718
- Sulentic J.W. & de Mello Rabaca D.F., 1993, ApJ 410, 520
- Tarchi A., Neininger N., Greve A. et al., 2000, A&A 358, 95
- Toomre A., 1964, ApJ 139, 1217
- Tran Q.D., Lutz D., Genzel R. et al., 2001, ApJ 552, 527
- Turner J.L., Ho P.T. & Beck S.C., 1998, AJ 116, 1212
- Ulvestad J.S., 1982, ApJ 259, 96
- Vader J.P., Frogel J.A., Terndrup D.M. & Heisler C.A., 1993, AJ 106, 1743

Vanzi L. & Rieke G.H., 1997, ApJ 479, 694

Wallace J.M., 1980, Ap&SS 68, 27

Walmsley M., 1995, RevMexAA S.C. 1, 137

Walsh D.E., Knapp G.R., Wrobel J.M. & Kim D.W., 1989, ApJ 337, 209

Welch G.A. & Sage L.J., 2003, ApJ 584, 260

Willmer C.N., Focardi P., da Costa L.N. & Pellegrini P.S., 1989, AJ 98, 1531

Woo J.H. & Urry C.M., 2002, ApJ 579, 530

Wunderlich E. & Klein U., 1988, A&A 206, 47

Yun M.S., Reddy N.A. & Condon J.J., 2001, ApJ 554, 803

Table 1. General data.

galaxy	J2000	group membership	$h_{75} D$ (Mpc)	$\Delta(cz)$ (km.s <sup>-1</sup> )	type	$D_{25}$ (arcmin)
NGC 1377	03 36 39.1 –20 54 07	Eridanus	21	$\approx +200$	amorphous <sup>a</sup>	1.78
IC 1953	03 33 41.8 –21 28 43	Eridanus	21	$\approx +280$	SBd	2.75
NGC 4491	12 30 57.2 +11 28 59	Virgo A	17	$\approx -550$	SBa dwarf <sup>b</sup>	1.70

<sup>a</sup>from Heisler & Vader (1994), who note the presence of a dust lane in the center.

<sup>b</sup>from Binggeli & Cameron (1983).

Table 2. Infrared and radio flux densities and derived quantities.

galaxy	$F_{100}$	$F_{60}$ (Jy)	$F_{25}$	$S_{1.4\text{GHz}}$ (mJy)	$L_{\text{FIR}}$ ( $10^9 L_{\odot\text{bol}}$ )	$L_{\text{FIR}}/L_{\text{B}}$	$F_{60}/F_{100}$	$q$
NGC 1377	5.97	7.27	1.92	$< 1.01^{\text{a}}$	4.3	3.3	1.22	$> 3.92 (8.1\sigma)$
IC 1953	11.62	9.01	1.05	$13.00^{\text{b}}$	6.1	1.6	0.78	$2.95 (3.2\sigma)$
NGC 4491	3.45	2.68	0.43	$< 1.35^{\text{c}}$	1.2	1.6	0.78	$> 3.41 (5.5\sigma)$

<sup>a</sup>This value is in agreement with the limit  $S_{1.49\text{GHz}} < 1.0 \text{ mJy}$  of Condon et al. (1990) measured in a  $21''$ -beam with the VLA.

<sup>b</sup>Our measurement on the NVSS map coincides with Condon et al. (1998).

<sup>c</sup>See Sect. 3.3 for an important discussion of this limit.

Table 3. Mid-infrared data.

galaxy	$F_{15\text{ tot}}$ (mJy)	$F_{7\text{ tot}}$ (mJy)	$D_{\text{CNR}}/D_{25}$	$D_{5\mu\text{Jy}}/D_{25}^{\text{a}}$	$F_{15\text{ CNR}}$ (mJy)	$F_{7\text{ CNR}}$ (mJy)	$(F_{15}/F_7)_{\text{CNR}}$
NGC 1377 <sup>b</sup>	$721 \pm 162$	$391 \pm 68$	0.22	0.88	705	343	$\approx 2.1$
IC 1953	$223 \pm 37$	$186 \pm 14$	0.09	0.79	116	34	3.4
NGC 4491	$81 \pm 25$	$31 \pm 8$	0.10	0.46	73	18	4.0

<sup>a</sup>Relative size of the isophote  $5\mu\text{Jy arcsec}^{-2}$  at  $7\mu\text{m}$ .

<sup>b</sup>The nucleus of NGC 1377 is slightly saturated both at 15 and  $7\mu\text{m}$ . The fluxes were measured on maps constructed by projecting together only the images which are not affected by saturation (since there is a shift of a non-integer number of pixels between each image, the brighter pixel receives a variable fraction of the flux of the central region). The total fluxes obtained without discarding the saturated images are  $F_{15\text{ sat}} = 705\text{ mJy}$  and  $F_{7\text{ sat}} = 366\text{ mJy}$ .

Table 4. Single-dish radio continuum fluxes.

	$S(3.6\text{ cm})$ (mJy)	$S(6.2\text{ cm})$ (mJy)	$S(21\text{ cm})$	$\alpha(3\text{--}6\text{ cm})^{\text{a}}$
beam size	$82''$	$147''$	$45''$	
NGC 1377	$< 2.0(3\sigma)$	$< 2.7(3\sigma)$	$< 1.0$	
IC 1953	$3.6 \pm 2.2^{\text{b}}$	$5.1 \pm 1.1^{\text{c}}$	13.0	$-0.64 \pm 1.19$
NGC 4491	$5.0 \pm 0.3$	$6.0 \pm 0.8$	$< 7.9^{\text{d}}$	$-0.34 \pm 0.27$
NGC 4418	$19.7 \pm 1.2$	$33.3 \pm 1.3$	$47.9 \pm 1.8$	$-0.97 \pm 0.13$

<sup>a</sup>Spectral index between 3 cm and 6 cm ( $S \propto \nu^\alpha$ ).

<sup>b</sup>Including the southern extensions (the noise in the map is  $0.6\text{ mJy/beam}$ ).

<sup>c</sup>The emission is extended, and the noise in the map is  $0.5\text{ mJy/beam}$ .

<sup>d</sup>See text (Sect. 3.3).

Table 5. PIFS spectroscopy.

line	date	$T_{\text{int}}^{\text{a}}$ (min)	airmass	line flux ( $10^{-18} \text{ W m}^{-2}$ )	continuum ( $10^{-15} \text{ W m}^{-2} \mu\text{m}^{-1}$ )	area
NGC 4491:						
Pa $\beta$	Feb. 1	80	$\approx 1.1$	$4.25 \pm 1.27$	18.9	$5.67'' \times 5.67''$
Pa $\beta$				$2.05 \pm 0.21$	3.09	$2'' \times 2''$
[FeII]	Feb. 2	133	1.1–1.3	$< 0.22 (3\sigma)$	1.66	$2'' \times 2''$
Br $\gamma$	Feb. 2	40	1.4–2.0	$0.56 \pm 0.24$	0.95	$2'' \times 2''$
NGC 4102:						
Pa $\beta$	Feb. 1	20	1.1–1.2	$120.8 \pm 4.8$	131.8	$4.83'' \times 4.83''$
[FeII]	Feb. 1	20	$\approx 1.1$	$76.7 \pm 3.2$	123.6	$4.83'' \times 4.83''$
Br $\gamma$	Feb. 2	20	1.6–1.8	$60.1 \pm 6.5$	117.2	$4.83'' \times 4.83''$
NGC 1377:						
Pa $\beta$	Oct. 17	26	1.7–1.8	$< 0.22 (3\sigma)$	4.51	$2'' \times 2''$
[FeII]	Oct. 17	26	1.7–1.8	$< 0.29 (3\sigma)$	3.96	$2'' \times 2''$
Br $\gamma$	Oct. 18	39	1.7–1.9	$< 0.47 (3\sigma)$	3.05	$2'' \times 2''$
H <sub>2</sub> 2.12	Oct. 18	35	1.7–1.8	$4.59 \pm 0.78$	7.34	$5.17'' \times 5.17''$
H <sub>2</sub> 2.25	Oct. 19	26	1.7–1.8	$< 0.14 (3\sigma)$		$2'' \times 2''$
H <sub>2</sub> 2.22	Oct. 19	30	1.7–1.8	$< 0.33 (3\sigma)$		$2'' \times 2''$
NGC 1022:						
Pa $\beta$	Oct. 17	18	1.4–1.5	$19.3 \pm 0.4$	13.9	$2'' \times 2''$
[FeII]	Oct. 17	15	1.3–1.4	$8.96 \pm 0.69$	12.1	$2'' \times 2''$
Br $\gamma$	Oct. 18	15	1.7–1.9	$8.14 \pm 0.35$	8.46	$2'' \times 2''$
H <sub>2</sub> 2.12	Oct. 18	40	1.4–1.7	$3.77 \pm 0.17$		$2'' \times 2''$
H <sub>2</sub> 2.25	Oct. 19	15	$\approx 1.3$	$0.72 \pm 0.17$		$2'' \times 2''$

<sup>a</sup>Total on-source integration time (an equal time was spent on the sky).



Table 6. SFR estimates.

galaxy	SFR <sub>CNR</sub> (7 μm)	SFR <sub>tot</sub> (FIR) (M <sub>⊙</sub> .yr <sup>-1</sup> )	SFR <sub>CNR</sub> (H)
NGC 1377 <sup>a</sup>	1.84	1.79	not applicable
IC 1953	1.65 ± 0.60	1.83	ext. Hα: 0.02 <sup>b</sup>
NGC 4491	0.3 ± 0.1	0.38	Paβ-Brγ: 0.04 <sup>c</sup>

<sup>a</sup>The star formation rates derived from the dust emission may be overestimates, due to various reasons (see text).

<sup>b</sup>From the (Hα + [NII]) flux measured on the map given by Antonio García-Barreto (uncorrected for extinction), with an approximate calibration based on the I-band measurement of Giovanelli et al. (1997), and after correcting for a slight over-subtraction of the continuum with the help of the I-band image, assuming the light follows the same distribution in I and in R.

<sup>c</sup>In 5.67'' × 5.67''.

Table 7. Far-infrared spectroscopy.

galaxy	[CII] 157.7	[OI] 63.2	[NII] 121.9	[OIII] 88.4
		(10 <sup>-16</sup> W m <sup>-2</sup> )		
NGC 1377 <sup>a</sup>	< 1.95	< 2.82	< 1.16	< 2.17
IC 1953 <sup>a</sup>	5.82 ± 0.40	< 2.82	< 1.44	< 4.31
NGC 4491 <sup>b</sup>	1.3			

<sup>a</sup>from Brauher (2002).

<sup>b</sup>from Leech et al. (1999).

Table 8. Molecular gas in NGC 1377.

	individual pointings ( $\Delta N$ , $\Delta E$ ) <sup>a</sup>				
	(0, 0)	(0, +1)	(0, +2)	(0, -1)	
	(-1, 0)	(+1, 0)	(-1, +1)	(-2, 0)	(-1, -1)
CO(1-0)	$1.62 \pm 0.11$	$1.64 \pm 0.09$	$< 0.9$	$1.48 \pm 0.12$	
	$1.67 \pm 0.12$	$1.42 \pm 0.12$	$1.10 \pm 0.15$	$< 0.11$	$< 0.73$
CO(2-1)	$1.91 \pm 0.06$	$1.85 \pm 0.08$	$< 0.6$	$0.98 \pm 0.09$	
	$2.32 \pm 0.08$	$1.25 \pm 0.09$	$< 0.26$	$< 0.22$	$< 0.10$
fitted model parameters:					
total CO(1-0) flux: $(1.75 \pm 0.12) \text{ K km s}^{-1}$					
total CO(2-1) flux: $(2.55 \pm 0.49) \text{ K km s}^{-1}$					
source FWHM: $(0 \pm 8) \text{ arcsec}$					
systematic pointing errors to obtain $\chi^2 = 1$ : $(+4, -2)$ , $(-5, 0)$ , $(-6, 0) \text{ arcsec}$ <sup>b</sup>					

<sup>a</sup>The offsets with respect to the center are given in units of  $11.5''$ , half the CO(2-1) beam width. All flux values,  $\int T_A^* dV$ , are in  $\text{K km s}^{-1}$ .

<sup>b</sup>One offset after each large rotation of the antenna (see Appendix B).

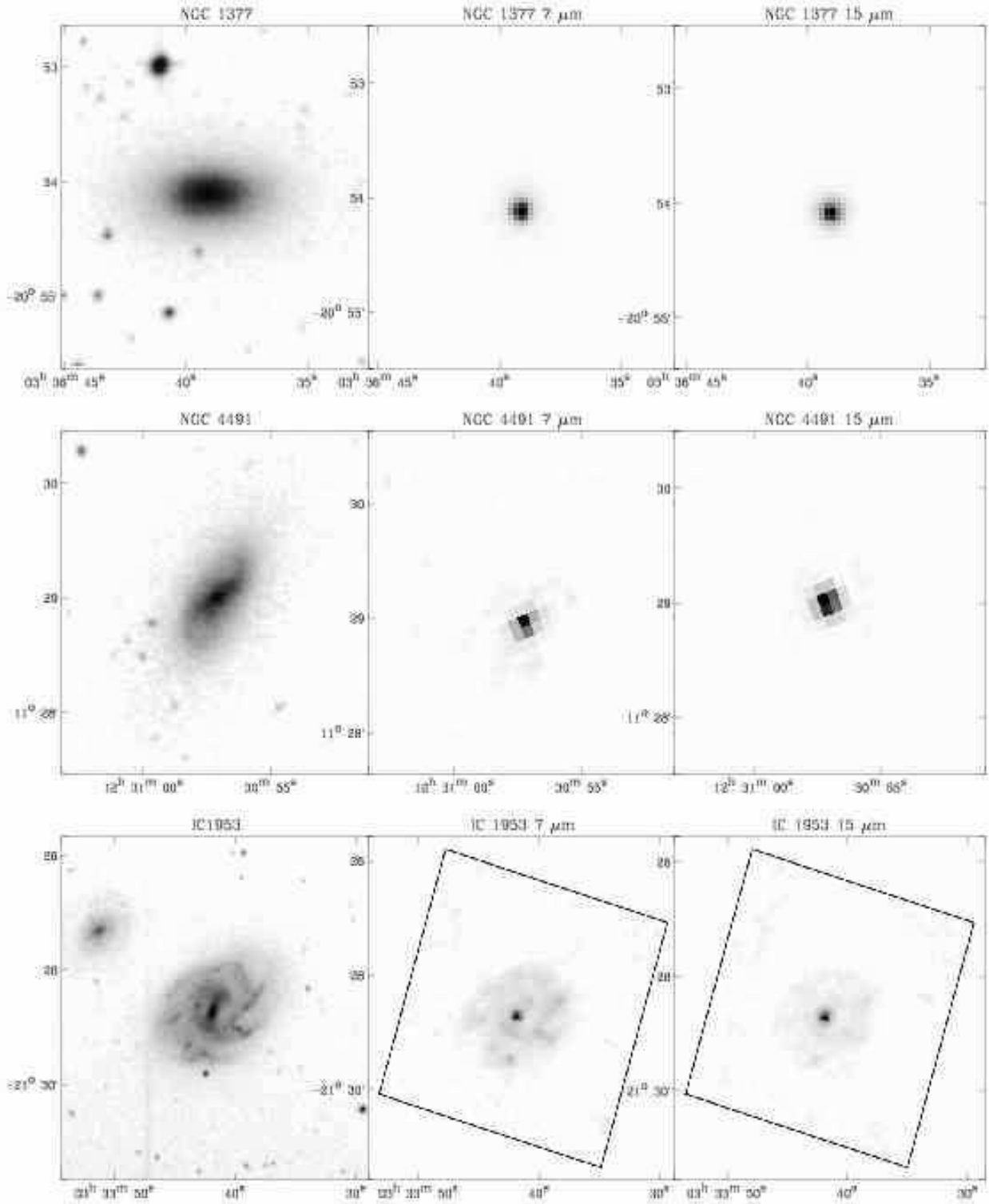


Fig. 1.— Red-band images from the DSS, and mid-infrared images in the bandpasses 5–8.5  $\mu\text{m}$  and 12–18  $\mu\text{m}$ .

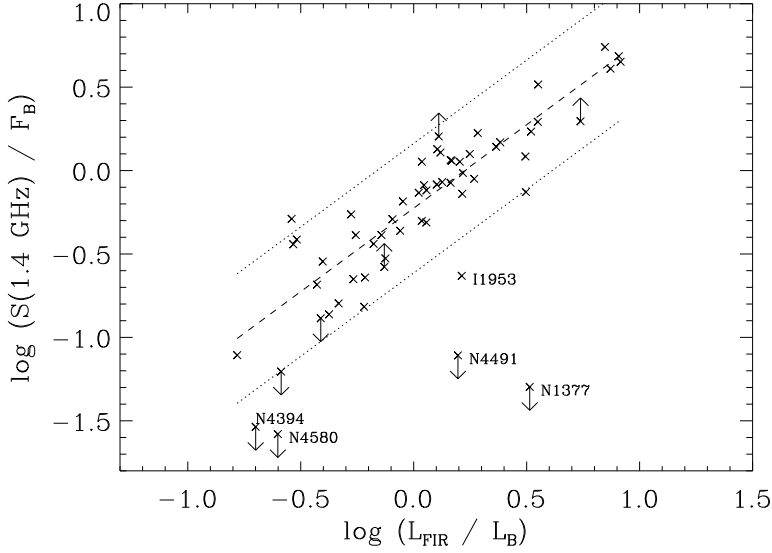


Fig. 2.— Correlation of radio and far-infrared fluxes, both normalized by the blue flux, in the sample of Roussel et al. (2001b) with the additional NGC 1377. The dashed line represents the average linear relation, and the dotted lines indicate the  $2\sigma$  interval of  $q$ . The galaxy with higher radio flux than  $\bar{q} - 2\sigma$  is NGC 4438, which has been disrupted by a collision, and the radio lower limit close to  $\bar{q} - 2\sigma$  is NGC 4388, a Seyfert galaxy. The galaxy at  $\bar{q} + 2\sigma$  with a high  $L_{\text{FIR}}/L_B$  ratio is NGC 1022, an amorphous starburst.

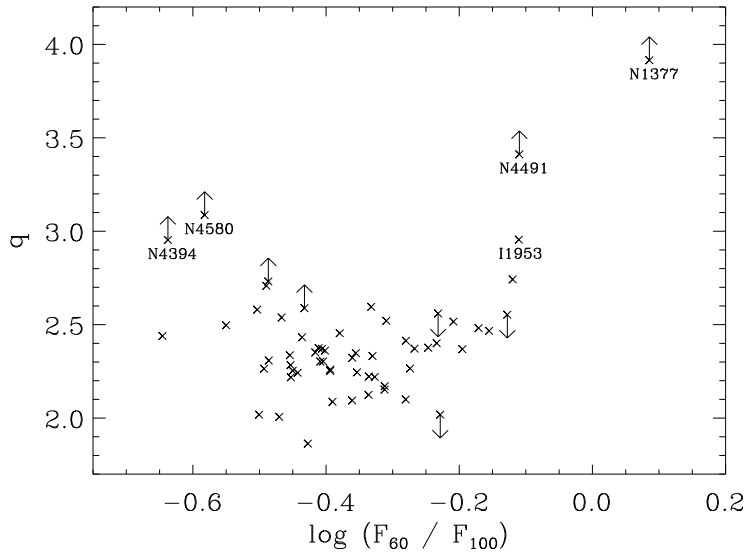


Fig. 3.— Logarithmic far-infrared to radio flux ratio as a function of  $F_{60}/F_{100}$ , indicating an average dust temperature.

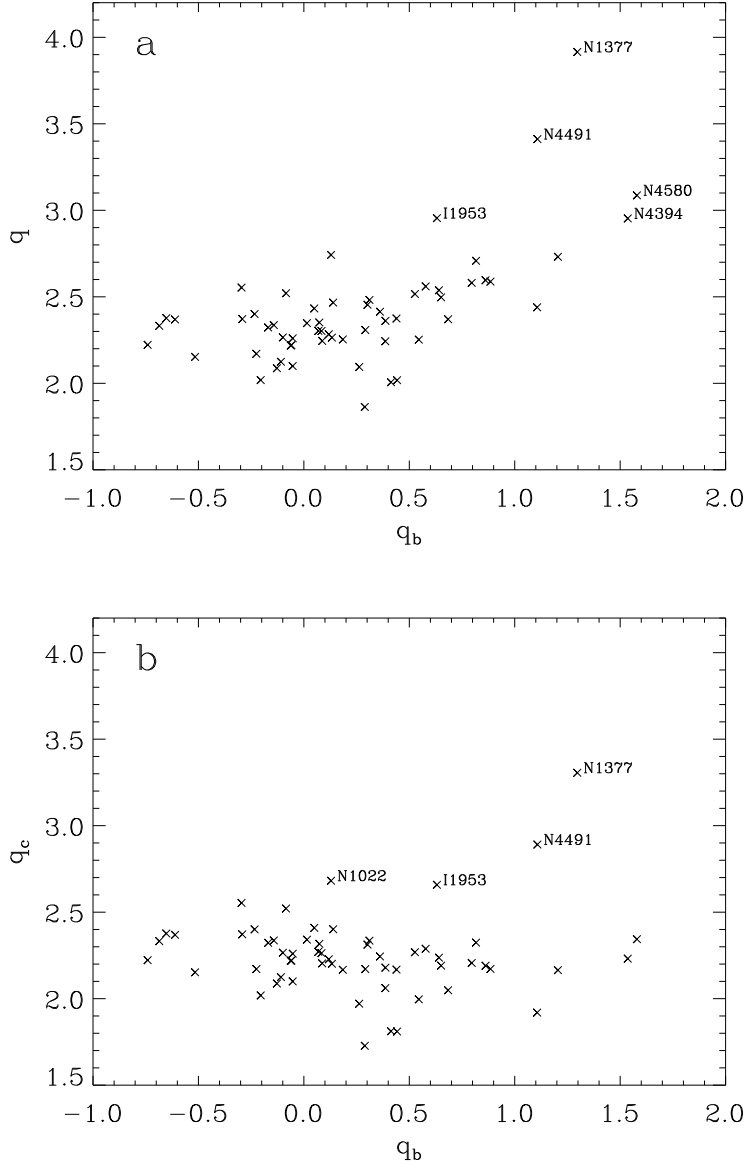


Fig. 4.— **a:**  $q$  as a function of  $q_b = \log(F_B/S(20\text{ cm}))$ , defined by Condon et al. (1991a) to linearize and tighten the radio-infrared correlation. **b:** Corrected infrared to radio ratio  $q_c$  as a function of  $q_b$ . The galaxies more than  $2\sigma$  above the average  $q_c$  are indicated.

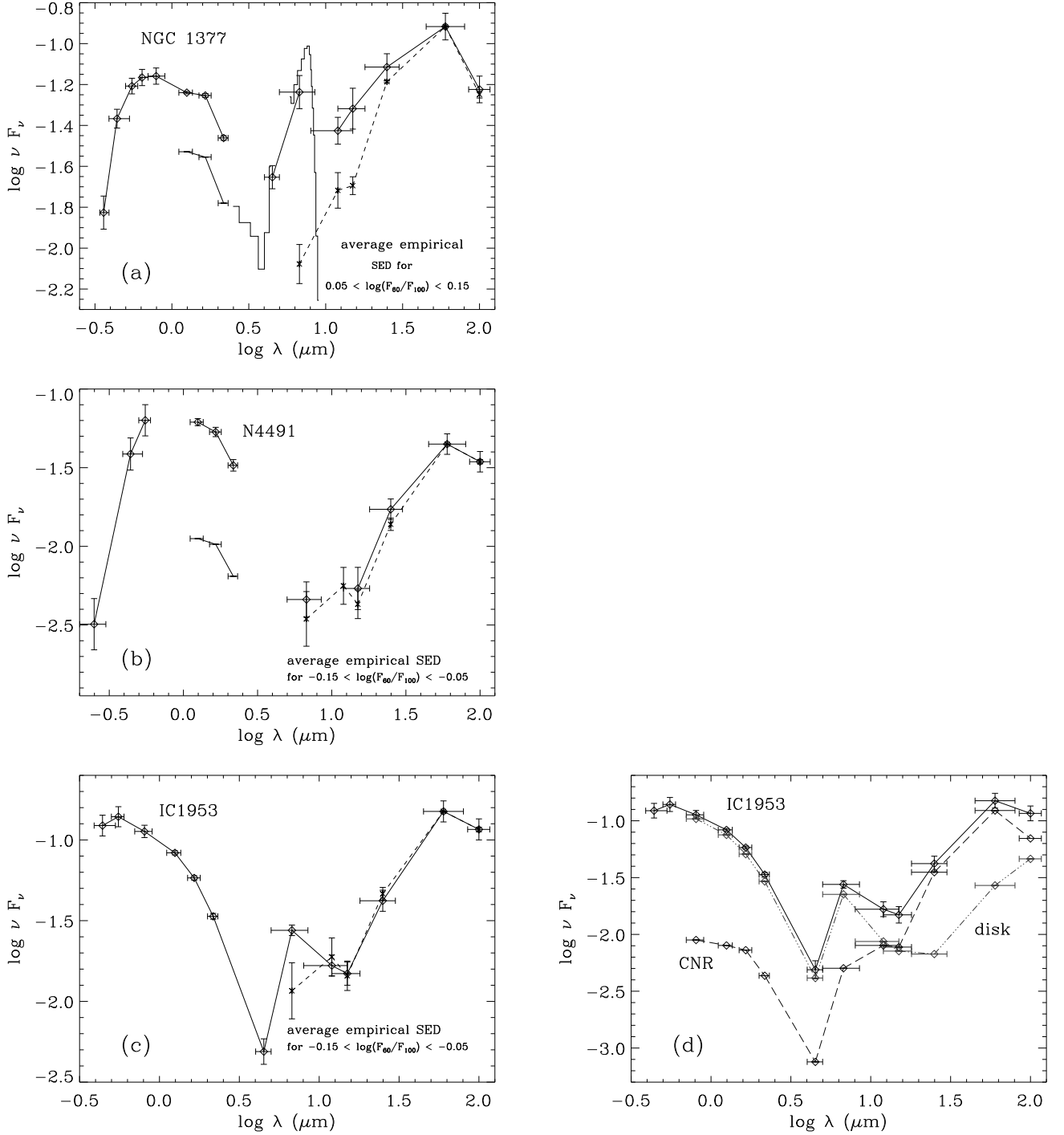


Fig. 5.— Spectral energy distribution (in arbitrary unit), compared with the average spectrum corresponding to the same  $F_{60}/F_{100}$  ratio from Dale et al. (2001) (dashed lines). The horizontal error bars represent the approximate filter widths. **(a)** The histogram superimposed on the SED of NGC 1377 reproduces the spectrum by Laureijs et al. (2000) in the  $[2.5; 4.8] \mu\text{m}$  and  $[5.8; 9] \mu\text{m}$  ranges. **(a) and (b)** The lower lines in the range  $\log \lambda \in [0.1; 0.35]$  correspond to the near-infrared spectra restricted to the mid-infrared emitting region. **(d)** The dot-dashed and dashed spectra are the decomposition of the SED of IC 1953 into the disk and the circumnuclear region, respectively.

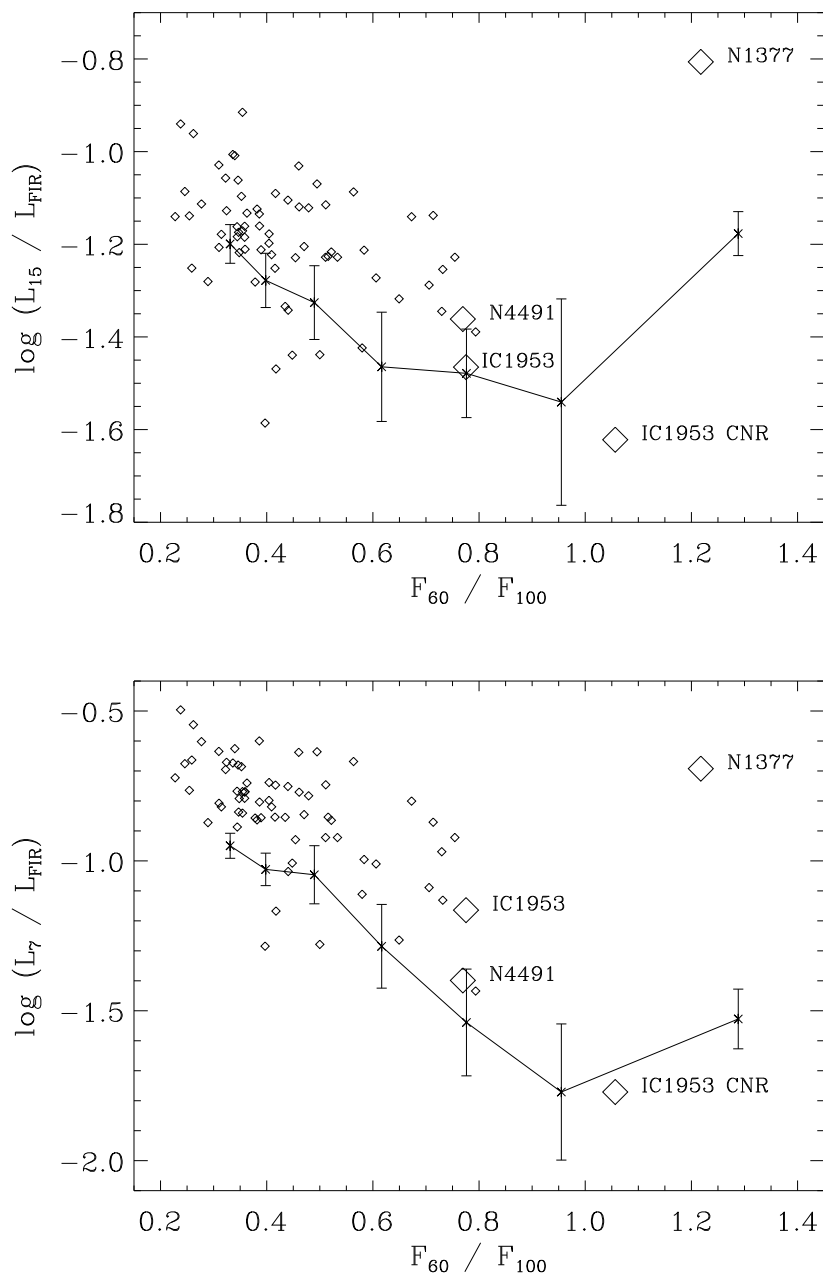


Fig. 6.— Mid-infrared to far-infrared luminosity ratios as a function of dust temperature in the sample of Roussel et al. (2001b) (small lozenges), average ratios of Dale et al. (2001) (dots connected with a line, with  $1\sigma$  dispersions), and ratios of NGC 1377, NGC 4491 and IC 1953 (big lozenges).

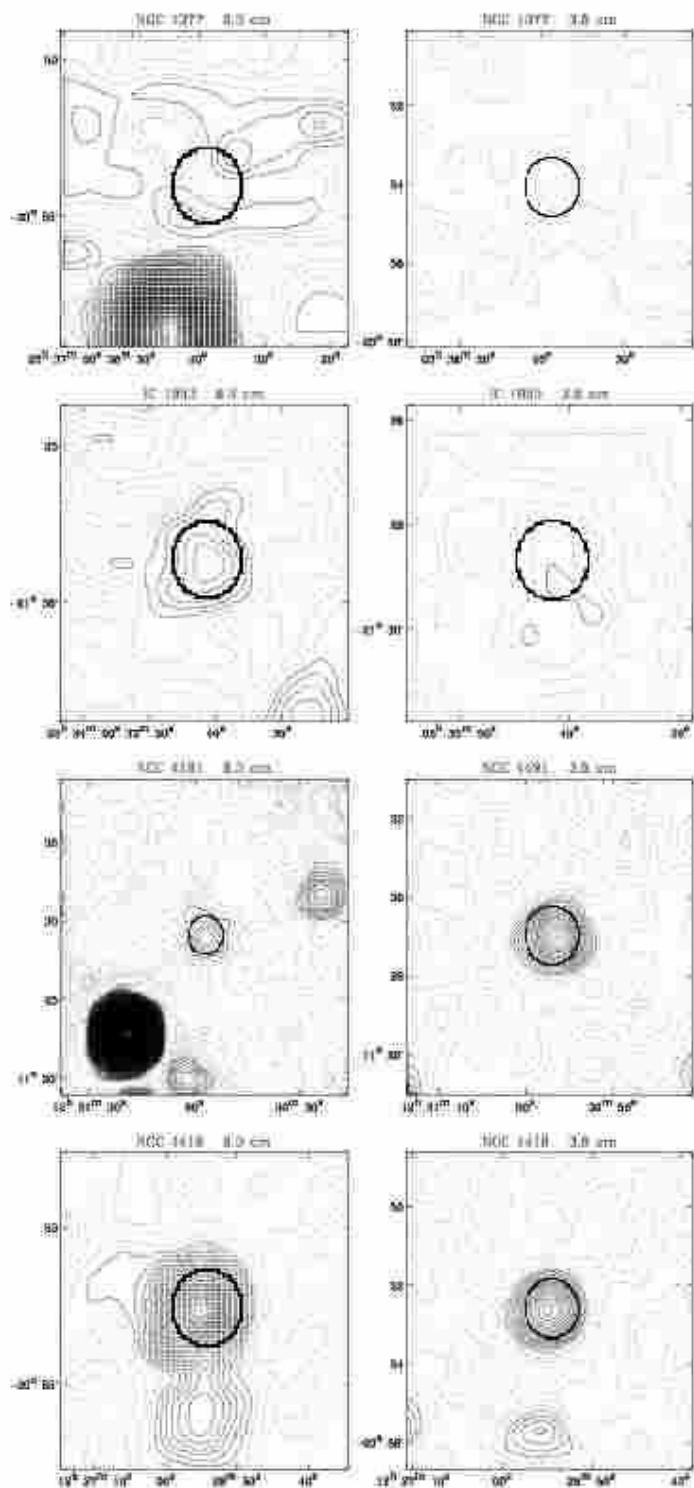


Fig. 7.— Contour maps at 6.2 cm (left) and 3.6 cm (right), spaced at  $1\sigma$ -intervals. The half-power beam width is indicated with a thick circle at the position of the galaxy. The continuous contours outline levels above  $3\sigma$ ; the grey dashed contours  $1\sigma$  and  $2\sigma$  levels; the dotted contours the zero level; to visualize any negative peaks which would indicate bad cleaning, the dot-dashed contours outline  $-1\sigma$  and  $-2\sigma$  levels (in grey), and  $-3\sigma$  (in black).



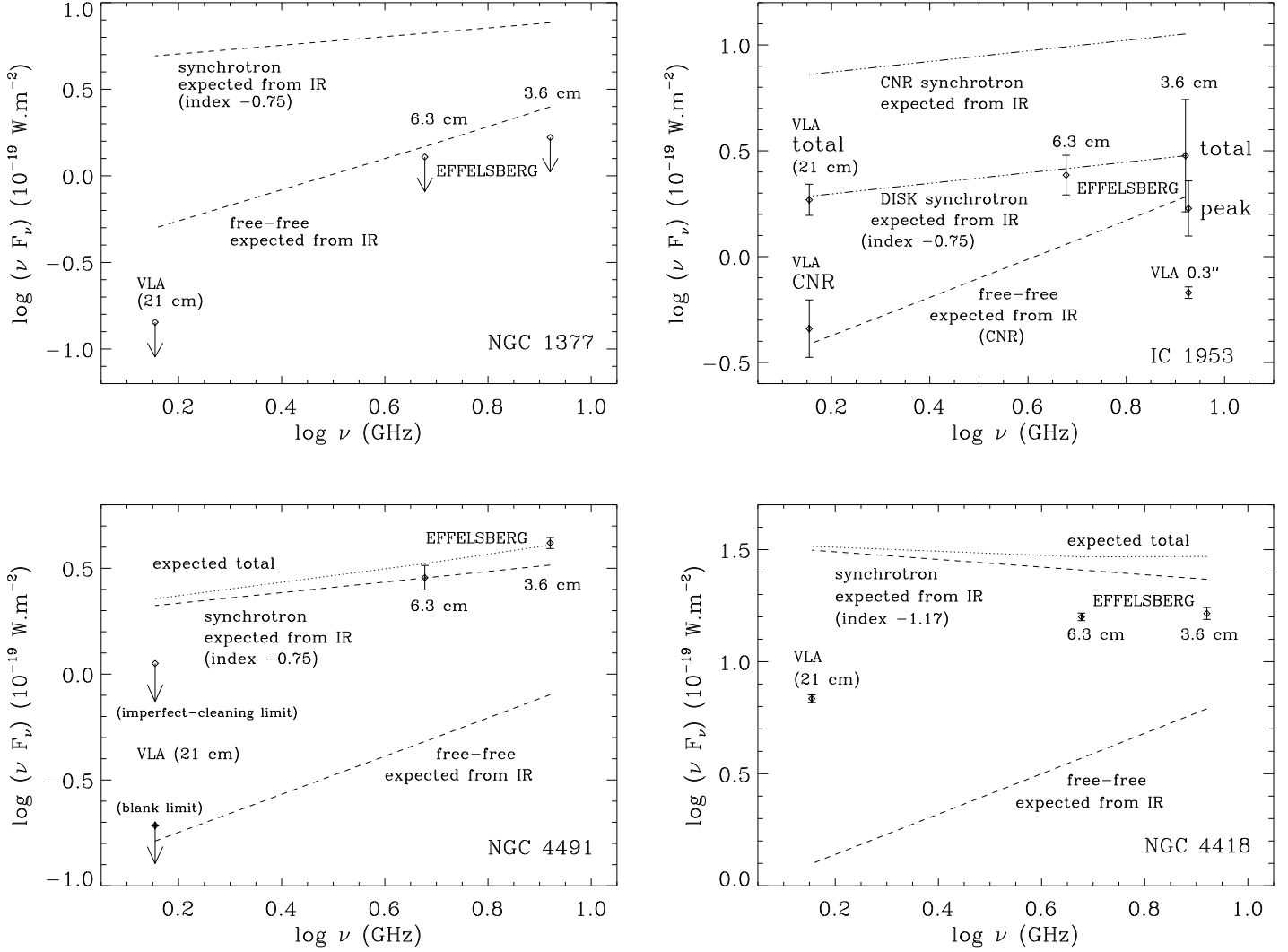


Fig. 8.— Radio continuum measurements. The dashed lines indicate the free-free and synchrotron emission expected from the far-infrared-derived SFR and the infrared-radio correlation followed by normal galaxies (with a thermal index  $S \propto \nu^{-0.1}$  and non-thermal indices indicated on the graphics). The radio spectrum of NGC 4418 is added here (see Section 6).

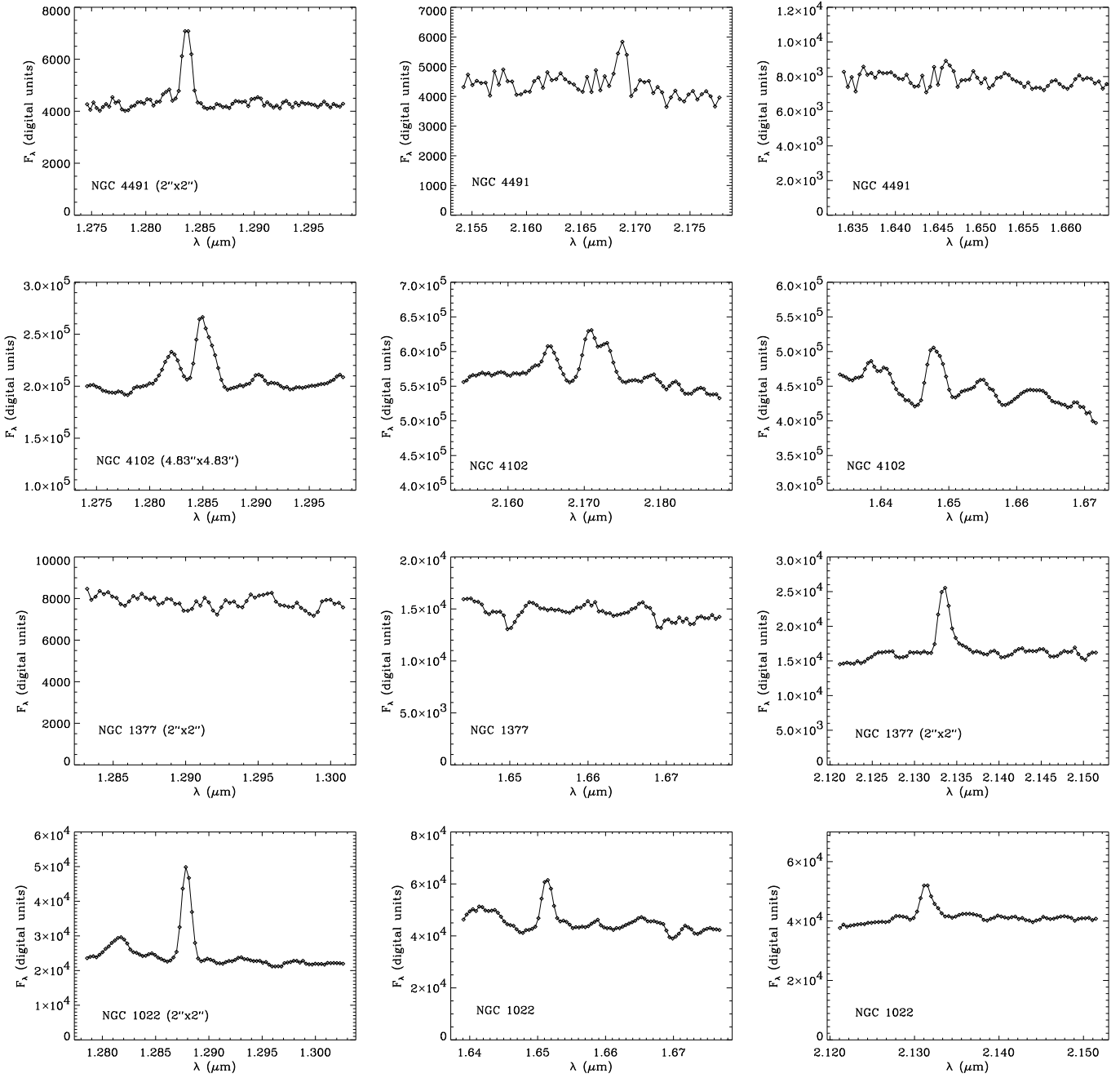


Fig. 9.— Near-infrared spectra of NGC4491 and the comparison starburst NGC4102 in the Pa $\beta$ , Br $\gamma$  and [FeII] 1.644 lines (in this order from left to right), and of NGC 1377 and the comparison starburst NGC 1022 in the Pa $\beta$ , [FeII] 1.644 and H<sub>2</sub> (1-0) S(1) lines. Since the line emission of NGC 4102 peaks slightly SE of the nucleus, the rotation broadening is asymmetric.

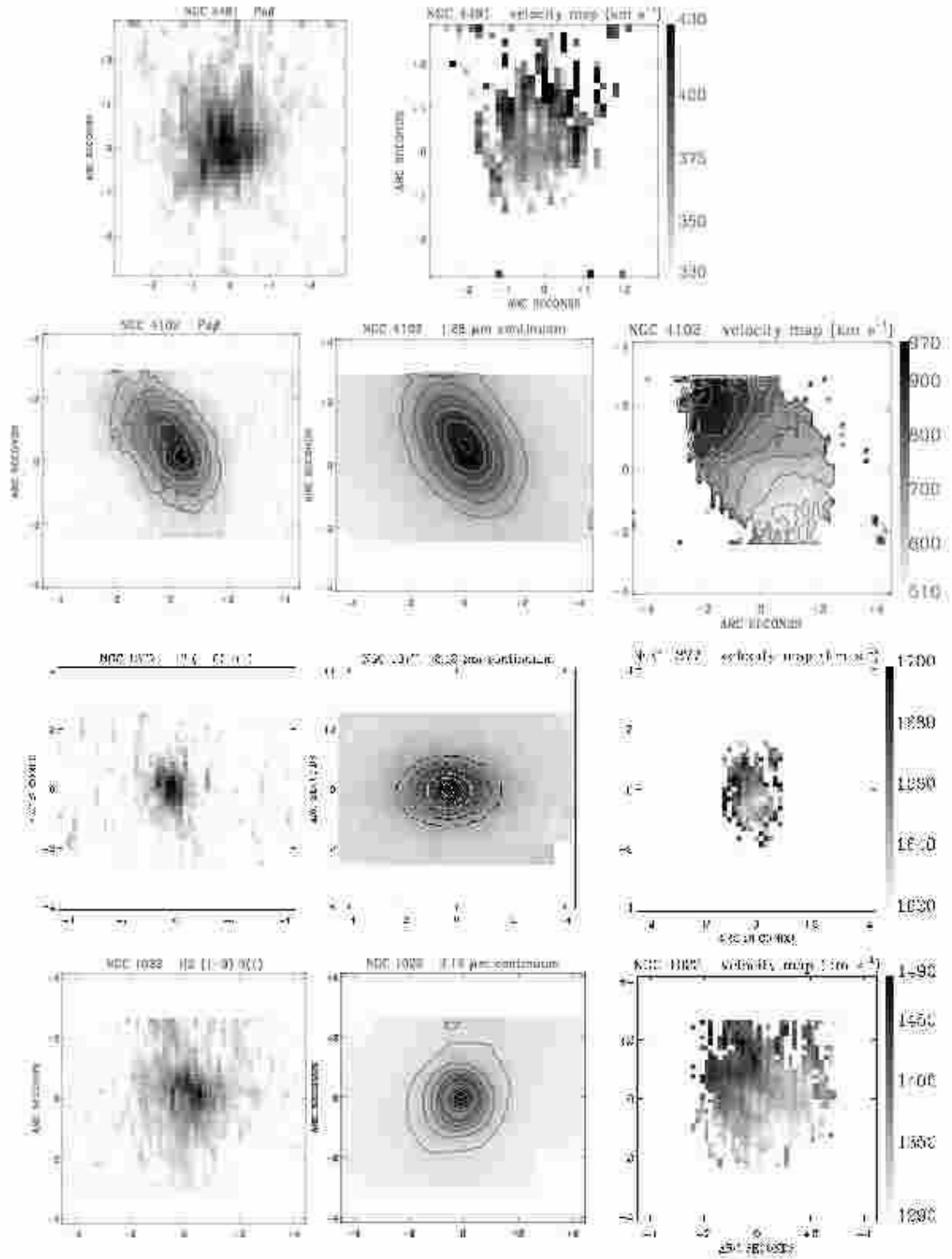


Fig. 10.— Continuum-subtracted images and velocity maps of NGC 4491 and NGC 4102 in the Pa $\beta$  line, and of NGC 1377 and NGC 1022 in the H<sub>2</sub> (1-0) S(1) line. The intensities range from 1 $\sigma$  to the maximum flux. Also shown are maps of the continuum emission around the line. The contours are equally spaced in flux and in velocity.

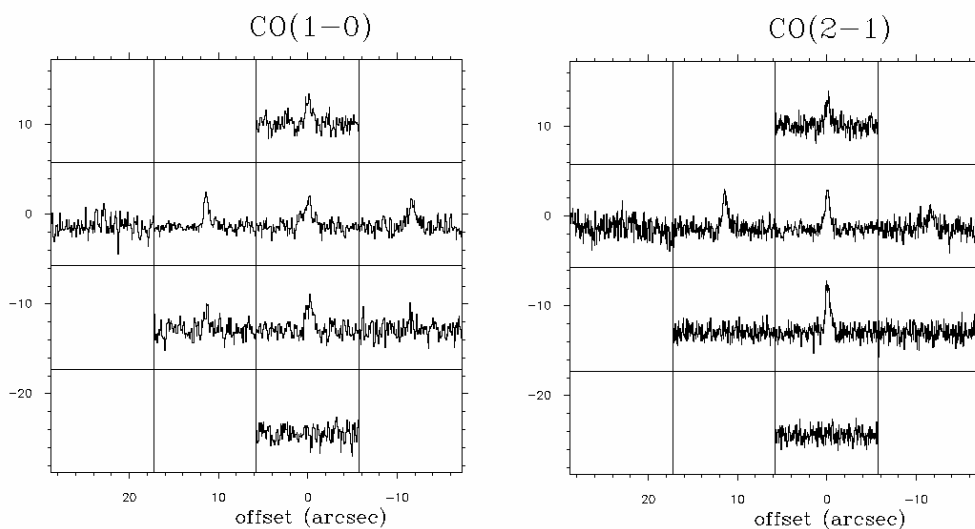


Fig. 11.— Averaged CO(1-0) and CO(2-1) spectra of NGC 1377 at the nine observed positions. The velocity range and temperature scale are the same for both lines, and the channel width was smoothed to four times the original width.

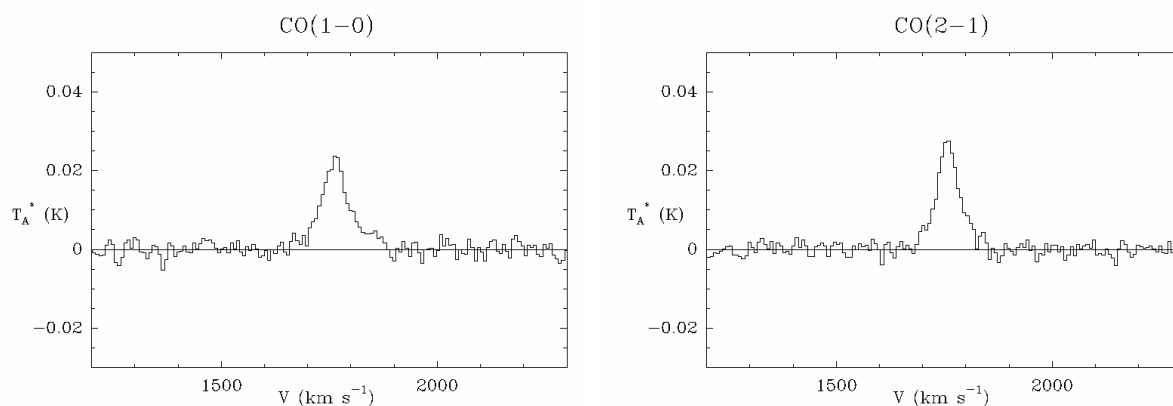


Fig. 12.— CO(1-0) and CO(2-1) spectra of NGC 1377 averaged over the five centermost positions. The channel width was Hanning-smoothed to about  $7.3 \text{ km s}^{-1}$  for both lines.